1 Marked-up manuscript version

2 Centennial to millennial climate variability in the far northwestern Pacific (off

3 Kamchatka) and its linkage to the East Asian monsoon and North Atlantic from the Last

4 Glacial Maximum to the Early Holocene

5 Sergey A. Gorbarenko [1], Xuefa Shi [2, 3], Min-Te Chen [4], Galina Yu. Malakhova, [5],

6 Aleksandr A. Bosin [1], Yanguang Liu [2, 3], Jianjun Zou [2, 3]

7 [1] V.I. Il'ichev Pacific Oceanological Institute, Russia

8 [2] Key Laboratory of Marine Sedimentology and Environmental Geology, First Institute of
9 Oceanography, SOA, Qingdao, China

10 [3] Laboratory for Marine Geology, Qingdao National Laboratory for Marine Science and
11 Technology, Qingdao, China
12 [4] National Taiwan Ocean University

13 [5] North-East Interdisciplinary Science Research Institute FEB RAS, Russia

14 Abstract

15 High resolution reconstructions based on productivity proxies and magnetic properties of core
16 LV63-41-2 (off Kamchatka) reveal prevailing centennial productivity/climate variability in the
17 northwestern (NW) Pacific from the Last Glacial Maximum (LGM) to the Early Holocene (EH).
18 The age model of the core is established by AMS ^{14}C dating and by projections of AMS ^{14}C data of
19 the nearby core SO-201-12KL through correlation of the productivity proxies and relative
20 paleomagnetic intensity. Resulted sequence of centennial productivity increases/climate warming
21 events in the NW Pacific occurred synchronously with the East Asian Summer Monsoon (EASM)
22 sub-interstadials during the LGM (4 events), Heinrich Event 1 (HE1) (4 events), Bølling/Allerød
23 (B/A) warming (4 events), and over the EH (4 events). Remarkable similarity of the sequence of the
24 NW Pacific increased productivity events with the EASM sub-interstadials over the LGM-HE1
25 implies that Siberian High is a strong common driver responded to the variations in productivity
26 and sub-interstadial. The comparison with the δ^{18}O record from Antarctica suggests that, another
27 mechanism associated with temperature gradient in the Southern Hemisphere may be also
28 responded for the EASM / NW Pacific centennial events over the LGM-HE1. During the B/A
29 warming and resumption of the AMOC, clear synchronicity between the NW Pacific, EASM and
30 Greenland sub-interstadials was mainly controlled by changes in the atmospheric circulation.
31 During the EH the linkages between sun-ocean-climate, likely, control the synchronicity of abrupt

climate changes in the NW Pacific and North Atlantic. The sequence of centennial events recorded in this study is a persistent regional feature during the LGM-EH, which may serve as a template in high resolution paleoceanography and sediment stratigraphy in the NW Pacific.

1. Introduction

Model simulations and proxy-based records both have led to contradictory results on the millennial-scale environmental variability in the northwestern (NW) Pacific and its underlying mechanisms during the last deglaciation. These model and proxy studies suggested either in-phase relationships of deglacial variability between the North (N) Atlantic and NW Pacific (Caissie et al., 2010; Chikamoto et al., 2012; Kienast and McKay, 2001; Seki et al., 2002) or out-of-phase responses (Gebhardt et al., 2008; Sarnthein et al., 2006). The in phase relationship has been attributed to rapid atmospheric teleconnections in the Northern Hemisphere on a decadal time scale (Max et al., 2012). The winter Arctic Oscillation (AO), which resembles the North Atlantic Oscillation, directly influences the surface air temperature and sea level pressure over the region northwards of 35ºN in East Asia (Sung et al., 2006). The Siberian High (SH), an essential component of northern East Asian atmosphere system, significantly influences the East Asian Winter Monsoon (EAWM) (Wu and Wang, 2002), which in turn affect the environment of NW Pacific. When winter AO is in its positive phase, both winter SH and EAWM are weaker than their normal state and air temperature of the surface- the middle troposphere is higher than normal (Wu and Wang, 2002), which ameliorate the NW Pacific environment. The out-of-phase response, however, was proposed to be driven by a seesaw mechanism, with oceanic readjustments between the weakening of the Atlantic meridional overturning circulation (AMOC) and the strengthening of the Pacific meridional overturning circulation (Okazaki et al., 2010).

Records of δ^{18}O from the Greenland ice cores revealed the Dansgaard - Oeschger (DO) millennial scale oscillations (interstadials and stadials) during the last glaciation (Dansgaard et al., 1993; Johnsen et al., 1992) and similar millennial scale events have also been identified in a number of terrestrial and marine records in other regions. For example, a synthesis of the last glacial pollen records from the European continent provides evidence that the warmer intervals in Europe correspond to millennial-scale interstadials in Greenland (Fletcher et al., 2010). The sediment cores from the N Pacific and its marginal seas also showed abrupt, millennial scale climate and environment ameliorations, similar to interstadials in Greenland ice cores during the last glaciation. Records of δ^{18}O of planktic foraminifera (Kennett et al., 2000) and alkenone-derived sea surface temperature (SST) (Seki et al., 2002) from the Northeastern (NE) Pacific also exhibited millennial climate oscillations very similar in magnitude with DO cycles over the last glaciation. INTIMATE stratigraphy studies introduced the subdivision of the GI-1 into sub-interstadials GI-1a to GI-1e.

66 Furthermore, the GS-2.1 was subdivided into sub-stadials GS-2.1a (during Heinrich Event 1, HE1),

67 GS-2.1b (Last Glacial Maximum, LGM), and GS-2.1c (Björck et al., 1998; Rasmussen et al., 2014).

68 The sequence of abrupt warming and environmental ameliorations similar to DO interstadials in

69 Greenland were also interpreted by using alkenone-derived SST (Harada et al., 2008) and

70 geochemical, diatom and pollen data (Gorbarenko et al., 2004) in sediment cores investigated from

71 the Okhotsk Sea. The Bering Sea was also characterized by climate and environmental oscillations

72 corresponded to DO cycles based on productivity proxies, sediment density, opal content and

73 micropaleontological records (Gorbarenko et al., 2005; Kim et al., 2011; Riethdorf et al., 2013;

74 Schlung et al., 2013).

75 By comparing the dust content in the North Greenland Ice Core Project (NGRIP) ice core with

76 that of the dust record in a sediment core from the subarctic N Pacific, Serno et al. (2015)

77 demonstrated synchronicity of millennial scale changes in atmospheric circulation between the N

78 Pacific and the Greenland during the last 27 ka (Serno et al., 2015). Previous studies also found the

79 occurrence of increased export of productivity during the period of millennial scale climate and

80 environmental ameliorations, correlated with DO interstadials, in the Okhotsk and Bering Seas

81 (Gorbarenko et al., 2005; Kim et al., 2011; Riethdorf et al., 2013; Seki et al., 2004).

82 Recent studies on high-resolution and well-dated sediment cores from the subarctic NW

83 Pacific, the Okhotsk Sea, and the western Bering Sea show the variations in SST during the last

84 deglaciation similar to the NE Pacific and to the N Atlantic and Greenland temperature variability

85 (Caissie et al., 2010; Max et al., 2012; Seki et al., 2002). These studies suggest a close linkage to

86 deglacial variations in AMOC associated with rapid atmospheric teleconnection, which were

87 responsible for a quasi-synchronous SST pattern between the N Atlantic and N Pacific during the

88 last deglaciation.

89 Furthermore, a recent study by Praetorius and Mix (2014), based on multi-decadal-resolution

90 foraminiferal δ^{18}O records from the Gulf of Alaska, revealed a synchronicity of rapid climate shifts

91 between the N Atlantic/Greenland (NGRIP record) and the NE Pacific between 15.5 and 11 ka.

92 During the Holocene and HE1, inverse relationships between the N Atlantic and the N Pacific are

93 suggested by Praetorius and Mix (2014), while the short-term variability is either not sufficiently

94 resolved or decoupled.

95 A lack of high resolution records in the NW Pacific prohibits a precise assessment of any

96 possible climatic teleconnection between the N Pacific and N Atlantic.

97 Besides centennial-millennial oscillations reported during the last glacial periods, centennial

98 precipitation anomalies from LGM to the Holocene have also been reported in cave stalagmite δ^{18}O

99   records of the East Asian monsoon (Dykoski et al., 2005; Wang et al., 2001, 2005, 2008; Yuan et

100   al., 2004). Furthermore, the timing and pattern of variability during the Early Holocene (EH)

101   regional climate changes are still under debate. In particular, though the EH climate has started

102   from a strong warming in most cases, a Hani peat δ^{18}O record from NE China instead suggest

103   centennial cooling event which is primarily superimposed on a long-term warming trend during the

104   Holocene (Hong et al., 2009).

105   Here we present high resolution results of productivity proxies, sediment magnetic properties,

106   and lithological composition of a sediment core LV 63-41-2 (hereinafter, 41-2) (off Kamchatka)

107   from the NW Pacific. Our records reveal a sequence of centennial productivity/climate variability

108   from 20 ka to 8 ka. An age model of core 41-2 was constructed using accelerator mass spectrometry

109   (AMS) ^{14}C dating and by correlating the productivity events and relative paleomagnetic intensity

110   (RPI) variability with those of the well-dated nearby core SO-201-12KL (hereinafter, 12KL) (Max

111   et al., 2012, 2014). Using robust age controls, we establish a tight linkage between the centennial

112   events with higher productivity in the NW Pacific and the sub-interstadial strengthened East Asian

113   summer monsoon (EASM) expressed in cave stalagmite δ^{18}O records. These results enable further

114   investigation of any mechanisms in controlling the in phase relationships of the centennial

115   variability in the NW Pacific / EASM and those underlying the Greenland / N Atlantic and

116   Antarctic climate changes during the LGM through EH.

117   **2 Materials and methods**

118   Sediment core 41-2 (52°34′ N, 160°01′ E; water depth: 1924 m) was recovered from the NW

119   Pacific off Kamchatka Peninsula during the Russian-Chinese Joint Expedition on R/V "Akademik

120   M.A. Lavrentyev" in 2013. The length of the core is 467 cm. In order to establish the age model of

121   core 41-2, we also analyzed paramagnetic magnetization and chlorin content in core 12KL (53°59′

122   N, 162°23′ E), which has been dated well by Max et al. (2012, 2014).

123   **2.1 Coarse fraction**

124   The weight percentage of coarse fraction (CF; 63-2000 μm) was obtained at 1 cm interval after

125   wet sieving the sediment and calculated as a ratio of CF weight to the total weight of dry bulk

126   sediment.

127   Terrigenous materials are mainly transported by sea ice in the studied region and therefore the

128   CF and magnetic susceptibility (MS) of sediments (Gorbarenko et al., 2003, 2012; Lisitzin, 2002;

129   Sakamoto et al., 2005), can be used as a proxy for ice rafted debris (IRD). Semi-quantitative

130   estimates of terrigenous and volcanic particles (tephra) in the CF allow the determination of core

131   intervals with insignificant amounts of tephra, and therefore intervals with implications for CF and

132   MS as an IRD index. Semi-quantitative estimates of major components in the sediment CF,
133   including terrigenous and volcanic particles, benthic and planktic foraminifera shells, diatom
134   frustules, and radiolarian skeletons on a twelve-point scale, were made by using a microscope for
135   roughly estimating the proportions of different components in the sediment (Rothwell, 1989).

136   **2.2 Chlorin**

137   Chlorin content is assumed to reflect changes in primary surface ocean productivity, because
138   continental-derived chlorophyll contributes insignificantly to its composition in deep marine
139   sediment (Harris et al., 1996). The chlorin content in core 41-2 was measured by a Shimadzu UV-
140   1650PC spectrophotometer at 1 cm resolution, and at 2 cm resolution in core 12KL, respectively,
141   using same analytical reagents and pretreatment procedures proposed by Harris et al. (1996).

142   **2.3 Total organic carbon (TOC), calcium carbonate ($CaCO_3$), and color b***

143   Contents of TOC, $CaCO_3$, and biogenic opal in deep sea sediments are usually used as key
144   parameters to assess paleoproductivity (Berger et al., 1989; Narita et al., 2002; Prahl et al., 1989;
145   Seki et al., 2004). The color b* values correlate well with the changes in biogenic opal content in
146   sediment cores (Nürnberg and Tiedemann, 2004) and are widely used as a paleoproductivity proxy
147   in the NW Pacific and its marginal seas (Gorbarenko et al., 2012; Max et al., 2012; Riethdorf et al.,
148   2013).

149   Total carbon and inorganic carbon contents in core 41-2 were measured at every 2 cm
150   throughout the core by Coulometry using an AN-7529 analyzer (Gorbarenko et al., 1998). TOC
151   content was determined by calculating the difference between total carbon and inorganic carbon
152   content. Color b* index (psychometric yellow–blue chromaticness) was measured with 1 cm
153   resolution using a Minolta CM-2002 color reflectance spectrophotometer (Harada, 2006).

154   **2.4 Radiocarbon dating (AMS ^{14}C)**

155   AMS ^{14}C-ages were measured in monospecific samples of the planktic foraminifera
156   *Neogloboquadrina pachyderma* sinistral (*N. pachyderma* sin.) from the 125–250 μm fraction, and
157   benthic foraminifera *Epistominella pacifica*, and *Uvigerina parvocostata* from the 250–350μm
158   fraction of the core. The radiocarbon dating was performed by Dr. John Southon at the Keck
159   Carbon Cycle AMS Facility (UCIAMS) in the Earth System Science Department of the University
160   of California, USA.

161   The constant reservoir age (900 ± 250 yr) of the NW Pacific surface water (Max et al., 2012)
162   was adopted in this study to convert the ^{14}C data into calendar ages by using Calib Rev 6.0 (Stuiver
163   and Reimer, 1993) with Marine13 calibration curve (Reimer et al., 2013) to establish consistent

164 AMS ^{14}C chronologies between cores 41-2 and 12KL. When using benthic foraminifera for AMS

165 ^{14}C dating on the cores, an age difference of 1400 yrs is taken between coexisting benthic and

166 planktic foraminifera ages (Max et al., 2014).

2.5 Magnetic properties

168 RPI in response to variations in the Earth's magnetic field presents an independent

169 chronological instrument of marine and continental sediments (Channell et al., 2009), and are

170 widely used for sediment correlation and chronology determination (Kiefer et al., 2001; Riethdorf et

171 al., 2013). The sediment paramagnetic magnetization (PM) was formed in marine sediments in the

172 open NW Pacific by silicate, paramagnetic iron sulphide (FeS), and fine clay minerals, the main

173 part of which was transported from land as an eolian dust through atmospheric circulation by

174 westerly jets (Serno et al., 2015). Therefore, the sediment PM may serve as a proxy for the land

175 aridity and atmosphere circulation pattern changes in response to climate change. The volume MS

176 of sediments was mainly formed by ferromagnetic minerals delivered together with terrigenous

177 materials from adjacent land by sea ice, which is the main transport agent of clastic materials into

178 the NW Pacific and its marginal seas (Gorbarenko et al., 2003; Lisitzin, 2002; Sakamoto et al.,

179 2005).

180 The sediment magnetic properties were measured at 2.2 cm resolution in cores 41-2 and 12KL.

181 MS of these samples was measured by an AGICO MFK1-FA device. The characteristic of remanent

182 magnetization (ChRM) of the samples was measured in the same way by studying the stability of

183 natural remanent magnetization (NRM) in an alternative magnetic fields of up to 80-100 mT on the

184 basis of analysis of Zijderveld vector plots, using an AGICO LDA-3Adevice and rock-generator

185 AGICO JR-5a (Zijderveld, 1964). The module and direction of NRM were measured on a JR-5A

186 rock-generator after the stepwise demagnetization of reference samples by alternating magnetic

187 fields with vanishing amplitude (Malakhov et al., 2009). Ahysteretic remanent magnetization

188 (ARM) was generated using an AGICO AMU-1A device and measured using the JR-5A rock-

189 generator. The RPI of the studied core was determined by the normalization of the ChRM after

190 demagnetization at 20 mT by ARM (ChRM/ARM) (Tauxe, 1993). The sediment PM was measured

191 for each sample from curves of magnetic hysteresis by a J Meter coercitive spectrometer at Kazan

192 State University, Kazan, Russia (Enkin et al., 2007; Jasonov et al., 1998).

2.6 In-situ X‑ray fluorescence core scanning

194 Previous studies have shown that the non-destructive, high resolution X-ray fluorescence

195 (XRF) measurements of biogenic barium, bromine and silica (Ba-bio, Br-bio, and Si-bio,

196 respectively) by a core scanner or synchrotron radiation are consistent with analytically measured

contents of Ba-bio, TOC, and biogenic opal, respectively, and therefore may be used as paleoproductivity proxies (Goldberg et al., 2005; Nürnberg and Tiedemann, 2004; Riethdorf et al., 2016). Ba-bio is formed during the decay of organic matter in the water column and the uptake of Ba in settling particles (Dymond et al., 1992), and has been previously used as a proxy of productivity (Goldberg and Arrhenius, 1958; McManus et al., 1998). Si-bio, related with biogenic opal in deep sea sediments, is usually used as a key parameter to assess paleoproductivity (Berger et al., 1989; Narita et al., 2002; Seki et al., 2004). Br-bio content measured using a core scanner is strongly correlated with TOC variability (Riethdorf et al., 2013) and therefore may also be used as a paleoproductivity proxy.

The elemental composition of core 41-2 was measured as peak area in counts per second at 0.5 cm resolution using the Itrax XRF core scanner at the First Institute of Oceanography, State Oceanic Administration, China. The Itrax XRF core scanner was set at 20 s count times, 30 kV X-ray voltage, and an X-ray current of 20 mA. Though absolute elemental concentrations are not directly available from the micro-XRF measurements, the count values can be used as estimates of the relative concentrations. The count values may be influenced by changes in the physical properties of the sediment, such as the water content and surface roughness of the core (Röhl and Abrams, 2000). However, the grain size of the 41-2 core is rather fine and the surface has been processed to be as flat as possible to minimize any effects from changing physical properties or roughness during the scanning.

In this study, attention was paid to the XRF scanning results for estimating the productivity proxies such as Ba-bio, Br-bio and Si-bio contents in our sediment core. The content of Ba-bio was estimated by the subtraction of its terrigenous component from the total Ba concentration in sediment (Ba-tot). The terrigenous component was, in turn, calculated from empirical regional $(Ba/Al)_{ter}$ ratios in the sediment core with the lowest Ba-tot contents multiplied on relative Al content:

Ba-bio = Ba-tot − $(Ba/Al)_{ter}$*Al (Goldberg et al., 2005).

The contents of Br-bio and Si-bio were calculated using the same way.

3. Results

3.1 Productivity events

Down-core variability of all productivity proxies (color b*and contents of TOC, chlorin, $CaCO_3$, Ba-bio, Si-bio, and Br-bio) in core 41-2 is presented Fig. 2. Taking the available AMS ^{14}C data into account (Table 1), the middle part of the core (the interval ~315-230 cm) with increased

229 contents/values of all productivity proxies could be chronologically assigned to the Bølling/Allerød

230 (B/A) warming right after the late last glaciation (467-315 cm) consistently with current

231 investigations. The climate became warmer in the northern extra-tropics during the B/A period,

232 terminating the last glaciation, then it reversed to the cooling during the Younger Dryas (YD)

233 followed by the significant warming throughout the Holocene. This climate sequence had been

234 well-documented by the $\delta^{18}O$ records of the Greenland ice cores and climate records from the N

235 Atlantic (Bond et al., 2001; Dansgaard et al., 1993; Johnsen et al., 1992; Stuiver et al., 1995), by

236 classical sequence of European pollen zone (Nilsson, 1983) and by well-dated pollen biome records

237 of the southern Siberia (Bezrukova et al., 2010; Tarasov et al., 2009). Above mentioned patterns of

238 climate variability during the LGM–EH in moderate-high latitudes of the Northern Hemisphere is

239 consistent with the N Pacific and its marginal seas, evidenced by the alkenone- derived SST (Barron

240 et al., 2003; Max et al., 2012) and pollen records (Gorbarenko et al., 2003, 2004). The significant

241 increase in productivity during the B/A was likely achieved by additional nutrient input into

242 euphotic layer due to accelerated sea level rise (Siddall et al., 2010) accompanied by the supply of

243 organic matter from the submerged shelf and by prolonged blooming season due to the warming

244 that is a common paleoceanography feature of the N Pacific and its marginal seas (Barron et al.,

245 2003, 2009; Caissie et al., 2010; Galbraith et al., 2007; Gorbarenko, 1996; Gorbarenko et al., 2005;

246 Gorbarenko and Goldberg, 2005; Keigwin, 1998; Keigwin et al., 1992; Max et al., 2012; Seki et al.,

247 2004). A decreased trend of productivity records at the interval of~230-190 cm is likely associated

248 with the YD cooling and the subsequent high productivity trend in the upper 190 cm of the core is

249 presumably related to the Holocene warming (Fig. 2).

250 In core 41-2, the temporal resolutions of measured color b*, chlorin, TOC, $CaCO_3$ and

251 magnetic parameters (PM, MS, and RPI), and Ba-bio, Br-bio, and Si-bio are nearly 30 years, 15

252 years, and 60 years respectively. The resolution is high enough to allow us to detect the centennial

253 scale productivity variability in the NW Pacific. However, not all productivity proxies change

254 synchronously (Fig. 2).

255 Each used productivity proxy has its own specific limitations and peculiarities in response to

256 the environmental and primary productivity changes. For example, although carbonaceous fossils

257 (planktic foraminifera and coccolithophorids) rain from the euphotic layer, exported by primary

258 production, and they provide the main carbonate input into the sediment. While the $CaCO_3$ content

259 in the deep sea sediment is mostly governed by climatically forced variability in the deep water

260 chemistry and carbonate ion concentration (CO_3^{2-}), resulting in different carbonate preservation in

261 the past (Yu et al., 2013). As for the Ba-bio proxy, Jaccard et al. (2010) suggest that in the highly

262 productive areas, barite dissolution has been observed under suboxic conditions, precluding its

application as a quantitative proxy to reconstruct past changes in export production. Although it has been suggested that biogenic opal and TOC contents are responsible for the accumulation of siliceous fossils, and siliceous plus carbonaceous fossils with other organic remains, respectively (Berger et al., 1989), they vary in different ways at various periods in sediments of the NW Pacific and its marginal seas. For example, biogenic opal content in the Okhotsk Sea lags significantly relative to TOC changes during the last deglaciation—the Late Holocene interval (Gorbarenko et al., 1998; Seki et al., 2004). TOC content in the hemipelagic sediment includes the organic carbon formed by marine primary production, and the terrigenous organic material delivered from land. Although it was suggested that color b* values correlate well with the changes in biogenic opal content in sediment cores (Nürnberg and Tiedemann, 2004), measured color b* in core 41-2 do not change synchronously with Si-bio content in the entire length of the core (Fig. 2). The presentation of a wide range of productivity records allows us to evaluate the discrepancy among proxies. In addition, the combination of proxies provides a more reliable way for evaluating the productivity changes.

For the statistical assessment of the centennial productivity variability, the stack of productivity proxies is calculated. It is an average of the normalized data of each proxy with equal weight (Fig. 2). Data from the productivity stack were detrended by subtracting long-term periodicity that allow us to determine the sequence of centennial productivity events with higher productivity throughout the studied core and events with lower productivity during the EH based on the seven productivity proxies measured (Fig. 2). Calculated productivity stack has high negative correlation with PM of sediments (r = -0.63). This indicates that centennial events with increased productivity occurred during weakening of dust delivery and deposition in the NW Pacific by atmospheric circulation associated with abrupt climate warming. Such causal linkages between centennial productivity increases and abrupt climate warming in the NW Pacific is also consistent with millennial scale productivity /climate oscillation during the DO interstadials found in the Okhotsk and Bering Seas (Gorbarenko et al., 2005; Kim et al., 2011; Riethdorf et al., 2013; Seki et al., 2004). As a result, the records of different productivity proxies and detrended productivity stack show eight short-term events with higher productivity occurred during the LGM and HE1 and 4 events during the B/A warming. During the EH, productivity records show 4 events of lower and higher productivity, respectively (Fig. 2).

It is noted that a low productivity event at ~9.1 ka (Table 1) is well-correlated with the 9.3 ka cold event recorded in NGRIP (Rasmussen et al., 2014). Moreover, a low productivity event identified at depth of 105-110 cm also correspond to the 8.2 ka cold event, a well-known chronostratigraphic marker in the Early to Middle Holocene boundary (Walker et al., 2012).

3.2. Age model

The RPI, productivity stack and PM of core 41-2 were compared with the RPI, several productivity proxies, and PM records of nearby core 12KL (Fig. 3). The color b* index and Ca (analog of $CaCO_3$ content) of core 12KL were obtained from Max et al. (2012, 2014). The correlation of the centennial productivity events between cores was provided by comparison of productivity stack of core 41-2 with productivity proxies of core 12KL and by comparison of the RPI and PM curves. An age model of core 41-2 was constructed using all available AMS ^{14}C data, with additional age control points identified by correlating the centennial productivity events, RPI and PM of the studied core with those of the well-dated adjacent core 12KL (Max et al., 2012, 2014) (Fig. 3). The age tuning used in this study assumes a synchronous pattern of productivity, RPI and PM variability in the NW Pacific since the last glacial, especially for closely-located cores. Therefore, the centennial variability of productivity proxies with increased productivity events, RPI of Earth's magnetic field, and PM identified in cores 41-2 and 12KL have to be closely matched in both cores over the last glaciation—B/A warming to the EH (Fig. 3). It was noted that the available age model for core 12KL (the Tiedemann/Max age model) (Max et al., 2012, 2014) was based on the AMS ^{14}C data and correlation of color b* index with the NGRIP $\delta^{18}O$ curve. For adopting this age model to Core 41-2, the AMS ^{14}C data of core 12KL were projected to Core 41-2 according to the correlation of related productivity events, RPI and PM (Fig. 3). The color b* minimum in core 12KL at a depth of 706 cm, which correlates with a minimum in the NGRIP $\delta^{18}O$ record at 16.16 ka, is also clearly correlated with the color b* minimum in core 41-2 at a depth of 348 cm (Fig. 3). All correlated AMS ^{14}C data points are also well-matched with the measured RPI curves of both cores (Fig. 3). Our four AMS ^{14}C data are fairly close to the projected ^{14}C data from core 12KL (Table 3) with age differences within ±0.1 ka, confirming the validity of these key point projections. Here the use of ^{14}C data of core 12KL is preferred, because this core has a higher sedimentation rate, and planktic foraminifera for these measurements were picked-up from intervals with higher Ca peaks, aiming to reduce the effect of bioturbation on the precision of age model.

A close temporal correlation of these NW Pacific increased productivity events with sub-interstadials in the EASM becomes apparent after projection of the radiocarbon data of both cores on absolute U-Th dated $\delta^{18}O$ record of Chinese cave stalagmites (Wang et al., 2008) during 20–8 ka (Fig. 3). Such inferred synchronicity of abrupt NW Pacific productivity events and EASM sub-interstadials was used for further tuning of age model. This was achieved by fine-tuning of the increased productivity events with related sub-interstadials of $\delta^{18}O$ Chinese stalagmites at a depth beyond the projected AMS ^{14}C data (Fig. 3; Table 3).

330   The sequence of centennial events of increased productivity seems to be occurred in phase

331   with decreasing of PM in both cores (Fig. 3), indicating a weakening of eolian dust transportation

332   by atmospheric circulation in the study area due likely to climate warming, analogous with

333   millennial scale forcing of dust transportation into the NW Pacific (Serno et al., 2015). Within the

334   constructed age model of core 41-2, different productivity proxies and magnetic records, combined

335   with similar data from core 12KL (Max et al., 2012, 2014) reveal a sequence of noticeable

336   centennial events of increased productivity in the NW Pacific which occurred in phase with Chinese

337   sub-interstadials (CsI) associated with stronger EASM or weaker EAWM (Wang et al., 2008) and

338   changes in atmospheric circulation during 21–8 ka (Figs. 3 and 4).

339   These linkages suggest that centennial increased productivity events in the NW Pacific were

340   likely associated with shifts of a warmer regional climate and/or higher nutrient availability in

341   surface water, synchronous with CsI of the EASM. According to Wang et al. (2001), the

342   interstadials of EASM are broadly correlated with regional climate warming. High resolution

343   records presented here show clearly that four centennial-scale events of increased

344   productivity/environmental amelioration correlated with CsI during the LGM, four events during

345   HE1, four events during the B/A warming, and four events during the EH (Fig. 4; Table 2).

346   **4. Discussion**

347   *4.1 Productivity patterns during the LGM-HE 1*

348   Besides the centennial productivity/environmental events, similar NW Pacific productivity

349   patterns are found in cores 41-2 and 12KL during the LGM and HE1 with some differences in

350   different productivity proxies. During the LGM, most proxies demonstrate a minimum primary

351   productivity in the NW Pacific without definite trends (Fig. 4). Severe environmental conditions in

352   central Asia inferred from pollen data (Bezrukova et al., 2010) (Fig. 5) seem to be promoted an

353   increase in winter sea ice formation and sea ice cover in NW Pacific, consistent with high IRD

354   accumulation inferred from CF and MS records (Fig. 4), that might have inhibited productivity in

355   the study area. It is also consistent with the minimum productivity in the NW Pacific due to strong

356   stratification, preventing the supply of nutrients required to support productivity in surface waters

357   (Gebhardt et al., 2008).

358   From 17.8 to 15.3 ka, the TOC and chlorin contents associated with the production of

359   calcareous phytoplankton (mostly coccolithophores) show a significant increase concurrently to the

360   diminished AMOC (McManus et al., 2004). The diminished AMOC resulted in a major cooling of

361   the Northern Hemisphere and, most likely, reduced water evaporation in the N Atlantic and

362   therefore Atlantic-Pacific moisture transport. This condition facilitates an overall increase in surface

water salinity, and decrease in surface stratification in the N Pacific, promoting an intensified ventilation of the intermediate water. The observed trends of productivity proxies are in concord with strong intensification of the intermediate-depth water ventilation in the N Pacific during HE1 (Max et al., 2014). However, fairly constant $CaCO_3$ values in both cores (water depth 1924–2145 m) during the LGM-HE1 do not indicate that the water ventilation penetrated to deep water in the N Pacific over that time interval, because carbonate concentration in the sediment is strongly constrained by the ventilation of bathed water (Yu et al., 2013). The productivity proxies such as Si-bio and color b*, associated with siliceous phytoplankton production (mostly diatoms), do not show significant trends during HE1 up to ~15.3 ka. The enhanced coverage of sea ice, shown by CF and MS records (Fig. 4), until 15.3 ka in the studied area probably lead to the overwhelmed production of diatom, due to the subsequent large spring–early summer surface water stratification. Both CF and MS records may represent IRD changes over the LGM-YD because the input of volcanic materials estimated in CF was insignificant during 21-12 ka compared to that of the Holocene (Fig. 4).

A sharp increase in the NW Pacific primary production, and a rise in the diatom production since ~15.3 ka indicated by most productivity proxies and Si-bio and color b* records with a peak at sub-interstadial GI1-e of B/A warming (Fig. 4), was likely induced by a decreased effect of sea ice and its spring melting, favoring a weakening of surface stratification. The timing of the decrease in the sea ice cover since ~15.3 ka is consistent with the regional surface water warming (Max et al., 2012). Such a pattern in productivity changes in the N Pacific and the Bering Sea during the glacial/interglacial transitions has been reported in previous studies (Caissie et al., 2010; Galbraith et al., 2007; Gebhardt et al., 2008; Gorbarenko, 1996; Keigwin, 1998) and was likely a persistent feature of the N Pacific and its realm, forced by the resumption of the AMOC at the B/A warming.

4.2 Centennial variations in productivity during the LGM-HE1-B/A

The identification of potential linkages between centennial climate changes in the Northern Hemisphere (NW Pacific, EASM, and N Atlantic/Greenland) and the climate changes recorded in the Antarctic ice cores is important for deepening our understanding of the mechanisms responsible for the timing and spatial propagation patterns that resulted from abrupt variability in global climate and environmental system. In order to test these linkages, the centennial productivity/climate events in the NW Pacific outlined by the productivity stack are compared with records from the Northern Hemisphere ($\delta^{18}O$ and Ca^{2+} of NGRIP, $\delta^{18}O$ of EASM, N Atlantic IRD, Siberian climate) and from the Southern Hemisphere (Fig.5). It has been suggested that the nearly synchronous ice core $\delta^{18}O$ and Ca^{2+} millennial-scale changes reflect the shifting of the Greenland atmospheric dust loading,

397 which is closely linked with the atmospheric circulation and climate changes in the high latitudes of
398 the Northern Hemisphere, where the EASM plays an important role (Ruth et al., 2007).

399   Similarity of glacial millennial-scale climate variability recorded in Chinese cave stalagmites
400 and Greenland ice cores (Sun et al., 2012; Wang et al., 2001) implies a plausible influence of high-
401 latitude climate of the Northern Hemisphere on the EASM by atmospheric circulation changes.
402 Several main elements of atmospheric circulation, including the Intertropical Convergence Zone
403 (ITCZ), northern westerly jet, AO and the SH, were previously considered as potential mechanisms
404 linking abrupt climate changes in the N Atlantic and East Asia (Jin et al., 2007; Nagashima et al.,
405 2011; Sung et al., 2006; Timmermann et al., 2007).

406   Apparent similarity of centennial climate and environment variability between the NW Pacific
407 productivity events, EASM and Greenland records (Fig. 5) allow us to suggest that mechanisms
408 responsible for their teleconnection were the same as on millennial scales. Remarkable similarity of
409 sequence of ~~the~~ NW Pacific productivity events with the sub-interstadials of EASM records during
410 the LGM-HE1 (Fig. 5) implies a strong common driver ~~responded to their variations~~. Wu and Wang
411 (2002) concluded that SH has provided direct and significant influence on the EAWM, particularly
412 by sea level pressure and northerly wind along the East Asian Coast. Simultaneously, the SH
413 strongly influences ~~on~~ the sea ice formation in the NW Pacific and marginal seas by ~~the~~ similar
414 mechanisms like the wind intensity controlled by pressure gradient and winter air temperature at ~~the~~
415 sea level (Kimura and Wakatsuchi, 1999). Records of CF and MS, related with IRD accumulation,
416 show that studied area off Kamchatka was ~~undergone to the~~ influence of sea ice during the LGM-
417 HE1 (Fig. 4). Enhancement of SH, associated with abrupt climate cooling, led to an increase in
418 terrigenous material delivery by sea ice from the coast and to a decrease in primary productivity by
419 shrinking of productive season between events with increased productivity.

420   Correlation of the centennial changes in the NW Pacific productivity events / CsIs with
421 Greenland sub interstadials during the LGM-HE1 was mainly observed but less clear, due to the
422 discrepancy in constructed age models / or to whatever differences in atmospheric teleconnections
423 (Fig. 5). There are some $\delta^{18}O$ differences between coeval $\delta^{18}O$ values in the Summit and NGRIP ice
424 cores during the LGM-HE1, which were likely controlled by changes in the N American Ice Sheet
425 volume and N Atlantic sea-ice coverage, resulting in the meridional discrepancy in the $\delta^{18}O$ of
426 Greenland ice (Seierstad et al., 2014).

427   EPICA community members (2006) showed that methane synchronization of the EDML and
428 the $\delta^{18}O$ of NGRIP reveal one-to-one alignment of each Antarctic warming with a corresponding
429 stadial in the Greenland ice cores, implying a bipolar seesaw mechanism on millennial time scales.

430   Since it was shown that Chinese and Greenland interstadials have occurred synchronously (Wang et

431   al., 2001), therefore, Chinese interstadials (CIs) were also, likely, related to the Antarctic cold

432   events. For example, warmer conditions at the Antarctic during 23.6–24.3 ka (coeval with Chinese

433   sub-stadial CsS-GS3-1) were synchronous with abrupt climate cooling and an increase in dust

434   content in the Greenland ice cores NGRIP, coeval with HE2 of the N Atlantic, and in phase with the

435   weakening of the EASM (GS/CS-3.1) (Fig.5). The Antarctic cooling after 23.4 ka was accompanied

436   by warming in Greenland, with two sharp interstadials GI-2.2 and GI-2.1 (Rasmussen et al., 2014)

437   and EASM interstadial CI-2 (Wang et al., 2001) (Fig. 5).

438   It has also been suggested that an index of monsoon intensity was controlled not only by the

439   Northern Hemisphere temperature ("pull" on the monsoon, which is more intense during boreal

440   warm periods), but also by the pole-to-equator temperature gradient in the Southern Hemisphere

441   ("push" on the monsoon, which is more intense during the boreal cold periods) that leads to

442   enhanced boreal summer monsoon intensity and its northward propagation (Rohling et al., 2009;

443   Rossignol-Strick, 1985; Xue et al., 2004). Since EASM transports heat and moisture from the West

444   Pacific Warm Pool (WPWP) to higher latitudes (Wang et al., 2001), the temperature gradient in the

445   Southern Hemisphere "pushes" the northward propagation of EASM via the latitudinal/longitudinal

446   migrations or expansion/contraction of the WPWP (Rohling et al., 2009; Xue et al., 2004). This also

447   explains the difference in responses to the EASM and Greenland interstadials and sub-interstadials,

448   because the migration of the WPWP may have occurred more slowly than the atmospheric

449   circulation changes (Rohling et al., 2009; Xue et al., 2004). The changes in the δ^{18}O records of

450   Chinese stalagmites were more gradual than in the δ^{18}O records of Greenland ice cores, and were

451   more similar to the changes of Antarctic air temperature (Fig. 5). So, it is possible that forcing from

452   low latitudes "push effect" on the EASM was additional mechanism in centennial productivity

453   changes in the NW Pacific due to surface water amelioration. Although time resolution of the

454   Antarctic δ^{18}O curve was not as high as ones from the Greenland and the EASM, records

455   demonstrated in Figure 5 do not exclude one-to-one alignment of each Antarctic centennial cooling

456   with related EASM sub-interstadial / NW Pacific productivity events.

457   We suggest that, in addition to the eight centennial productivity/environmental events during

458   the LGM-HE1 established in the studied cores from the NW Pacific, other three abrupt

459   productivity/climate events likely took place in the NW Pacific, synchronous with CsIs outlined by

460   the δ^{18}O records of Chinese stalagmites and the Greenland during the interval of 25–20 ka (namely

461   CsI-GS2.1-11, CsI-GS2.1-10, and CsI-GS2.1-9) (Fig. 5).

462   During the B/A warming and resumption of the AMOC, four sub-interstadials (CsI-GI1-a to

463   CsI-GI1-e) were clearly and simultaneously observed in the Greenland ice cores δ^{18}O (Björck et al.,

1998) and dust records and EASM sub-interstadials synchronously with centennial productivity / environment events of the NW Pacific (Fig. 5). It is consistent with enhancement of the "pull effect" on the intensified EASM and therefore amelioration of the NW Pacific during boreal warm period, which implies a dominant control of Northern Hemisphere climate processes on the atmospheric circulation in high latitudes (Rohling et al., 2009). Related significant coeval changes in the atmosphere circulation with periodicity *ca* 0.4 ka exert strong influence on the climate and environment in ocean and continent of the Northern Hemisphere during the B/A (Bezrukova et al., 2010).

4.3 Centennial variations in productivity during the EH

During the EH the records presented here show an alternation of the four NW Pacific centennial events with lower and four ones with higher productivity, namely as CsS-EH-1 -CsS-EH-4 and CsI-EH-1 - CsI-EH-4, respectively (Figs. 4 and 5; Table 2). The low productivity events (CsS-EH-1 and CsS-EH-2) are likely correlated with Greenland cold events at 8.2 ka and 9.3 ka, respectively (Rasmussen et al., 2014). Also, the NW Pacific low productivity events (CsS-EH-1, CsS-EH-2 and CsS-EH-3) occurred synchronously with the EASM decrease and whatever climate cooling recorded in $\delta^{18}O$ of the Dongge cave stalagmite D4 (Dykoski et al., 2005) (Fig. 5). Therefore it may be suggested that during the EH the NW Pacific events with higher / lower productivity had occurred coeval with climate warming / cooling as well. The pollen-based reconstruction of the variability of the vegetation / climate from a well-dated core from south Siberia (Lake Baikal region) (Bezrukova et al., 2010) demonstrated nearly the same pattern of centennial variability during the EH (Fig. 5). Well-dated, high resolution lithological and geochemical results from the Yanchi playa (NE China) also clearly showed a sequence of three sharp cooling events at 8.2 ka, 9.9–10.1 ka, and 11.0–11.2 ka (Yu et al., 2006), quasi-synchronous with the NW Pacific productivity / climate events CsS-EH-1, CsS-EH-3 and CsS-EH-4. Yu et al. (2006) explained this correlation through linkages between the tropical Pacific and N Atlantic.

An alternation of the NW Pacific events with lower / higher productivity during the EH demonstrates a perfect correlation with periodicities of solar activity and the production of the cosmogenic nuclides ^{14}C and ^{10}Be (Reimer et al., 2004) (Fig. 5). The production rates of these cosmogenic nuclides and residual atmospheric $\Delta^{14}C$ record are negatively correlated with total solar irradiance due to the strength of magnetic fields embedded into the solar wind (Hu et al., 2003). Small variations in solar irradiance could be responsible for pronounced changes in northern high-latitude climate and environments (Bond et al., 2001; Hu et al., 2003). The NW Pacific events of higher productivity occurred during increased solar irradiance and climate warming, indicating that variability of the solar irradiance was a potential driver of the climate and environmental changes in

the NW Pacific during the EH. The low productivity / cold climate CsS-EH-2 event in records of atmospheric Δ^{14}C and the Greenland δ^{18}O ice core was marked by sharp cooling at its onset and termination with some warming during the transition (Fig. 5). The CsS-EH-4 event shows a similar pattern in records of productivity stack and δ^{18}O of the Greenland and Dongge cave D4, indicating fine structure of these cold events.

The influence of variations in solar output on hydrography of surface ocean in the subpolar N Atlantic during the Holocene was reported by Bond et al. (2001). The variability of subpolar N Atlantic ice drifting, recorded as the percentage of hematite-stained grains (Bond et al., 2001), though having lower time resolution and dating precision compared with production of the cosmogenic nuclides, is consistent with other centennial climate changes in the Northern Hemisphere during the EH (Fig. 5).

The high resolution records of an alternation of the NW Pacific events with lower / higher productivity related with climate cooling / warming, demonstrating that centennial scale climate events during the EH were similar between the N Atlantic and NW Pacific, possibly because of the close linkages of sun-ocean-climate, consistent with earlier conclusions (Bond et al., 2001; Hong et al., 2009; Hu et al., 2003).

4.4 Cross-correlation of the N Atlantic-NW Pacific climate variability

Since whether N Atlantic-NW Pacific climate and hydrological in-phase or out-of-phase linkages are still under debate, empirical data obtained from sediment cores off Kamchatka offer the provision for clarifying this issue at high resolution. Here we provide comparison of the productivity stack of core 41-2, responsible for NW Pacific environmental variability, and δ^{18}O records of the NGRIP ice core, responsible for the Greenland / N Atlantic climate changes (Rasmussen et al., 2014). Cross correlation of these records using moving windows at 2000 years shows more significant synchronization (from -0.6 to - 0.9) from 15.8 ka up to 10.8 ka confirming strong atmospheric teleconnections between the NW Pacific and the N Atlantic during this period (Fig. 6). Cross correlation during early (19 ka - 15.8 ka) and later periods (10.8 ka - 9 ka) indicates weak NW Pacific - N Atlantic linkages, but do not support the out-of-phased hypothesis.

5. Conclusions

This study presents high resolution records of productivity proxies (TOC, CaCO$_3$, chlorin, color b*, Ba-bio, Br-bio and Si-bio), sediment lithological, and magnetic properties from sediment cores, 41-2 and 12KL, taken from the NW Pacific. Results presented here reveal 16 centennial regional productivity events during the LGM-EH (20–8 ka) in the NW Pacific. Four NW Pacific abrupt productivity increased events are linked to CsIs during the LGM (20–17.8 ka), four ~~ones~~

532 during HE 1 (17.8–14.7 ka) and four ~~ones~~ during the B/A. An alternative occurrence of four
533 centennial events with lower and higher productivity was established during the EH.

534 On the basis of age models of cores 41-2 and 12KL, we suggest that NW Pacific centennial
535 events of increased productivity occur synchronously with sub-interstadials of the EASM. These
536 NW Pacific events and EASM sub-interstadials are positively correlated with Greenland abrupt
537 warming, indicating an atmospheric teleconnection between the NW Pacific and the N Atlantic
538 during the LGM-HE 1-B/A.

539 Remarkable similarity of the sequence of productivity events recorded in the NW Pacific
540 with the EASM sub-interstadials during the LGM-HE1 implies that SH is a strong driver ~~responded~~
541 ~~to their variation~~. The comparison between our stacked productivity with the $\delta^{18}O$ of the EPICA,
542 NGRIP and EASM suggest that another mechanism associated with temperature gradient in the
543 Southern Hemisphere ("push~~es~~ effect") may be responded to the EASM sub-interstadials and
544 subsequent variability in productivity events in the NW Pacific on centennial time scale during the
545 LGM-HE1.

546 During the B/A warming and resumption of the AMOC, synchronicity between the
547 productivity events, EASM sub-interstadials, and the $\delta^{18}O$ and dust records in the NGRIP is
548 consistent with enhancement of the "pull effect" on the monsoon's intensity, which implies a
549 dominant control of atmospheric processes on the productivity and climate of the NW Pacific.

550 During the EH, the high resolution records of an alternation of productivity events with
551 lower / higher productivity related with climate cooling / warming, reveal that centennial climate
552 events were similar between the subpolar regions of the N Atlantic and NW Pacific, and were
553 controlled by mechanisms of sun-ocean-climate linkages.

554 In summary, the NW Pacific results presented here indicate a tight linkage and coherent
555 pattern of centennial - millennial scale climate changes during the LGM-EH, which may serve as a
556 template in high resolution paleoceanography and sediment stratigraphy of the moderate-high
557 latitudes in the NW Pacific.

558

Acknowledgements

References

571 Barron, J. A., Heusser, L., Herbert, T. and Lyle, M.: High-resolution climatic evolution of coastal
572 northern California during the past 16,000 years, Paleoceanography, 18(1),
573 doi:10.1029/2002PA000768, 2003.

574 Barron, J. A., Bukry, D., Dean, W. E., Addison, J. A. and Finney, B.: Paleoceanography of the Gulf
575 of Alaska during the past 15,000 years: Results from diatoms, silicoflagellates, and geochemistry,
576 Mar. Micropaleontol., 72(3–4), 176–195, doi:10.1016/j.marmicro.2009.04.006, 2009.

577 Berger, W. H., Smetacek, V. S. and Wefer, G.: Ocean Productivity and Paleoproductivity - An
578 Overview, in Productivity of the Ocean: Present and Past, pp. 1–34., 1989.

579 Bezrukova, E. V., Tarasov, P. E., Solovieva, N., Krivonogov, S. K. and Riedel, F.: Last glacial–
580 interglacial vegetation and environmental dynamics in southern Siberia: Chronology, forcing and
581 feedbacks, Palaeogeogr. Palaeoclimatol. Palaeoecol., 296(1–2), 185–198,
582 doi:10.1016/j.palaeo.2010.07.020, 2010.

583 Björck, S., Walker, M. J. C., Cwynar, L. C., Johnsen, S., Knudsen, K.-L., Lowe, J. J. and
584 Wohlfarth, B.: An event stratigraphy for the Last Termination in the North Atlantic region based on
585 the Greenland ice-core record: a proposal by the INTIMATE group, J. Quat. Sci., 13(4), 283–292,
586 doi:10.1002/(SICI)1099-1417(199807/08)13:4<283::AID-JQS386>3.0.CO;2-A, 1998.

587 Bond, G. C., Kromer, B., Beer, J., Muscheler, R., Evans, M. N., Showers, W., Hoffmann, S., Lotti-
588 Bond, R., Hajdas, I. and Bonani, G.: Persistent solar influence on North Atlantic climate during the
589 Holocene, Science, 294(5549), 2130–6, doi:10.1126/science.1065680, 2001.

590 Caissie, B. E., Brigham-Grette, J., Lawrence, K. T., Herbert, T. D. and Cook, M. S.: Last Glacial
591 Maximum to Holocene sea surface conditions at Umnak Plateau, Bering Sea, as inferred from
592 diatom, alkenone, and stable isotope records, Paleoceanography, 25(1), PA1206,
593 doi:10.1029/2008PA001671, 2010.

594 Channell, J. E. T., Xuan, C. and Hodell, D. A.: Stacking paleointensity and oxygen isotope data for
595 the last 1.5 Myr (PISO-1500), Earth Planet. Sci. Lett., 283(1–4), 14–23,
596 doi:10.1016/j.epsl.2009.03.012, 2009.

597 Chikamoto, M. O., Menviel, L., Abe-Ouchi, A., Ohgaito, R., Timmermann, A., Okazaki, Y.,

598 Harada, N., Oka, A. and Mouchet, A.: Variability in North Pacific intermediate and deep water
599 ventilation during Heinrich events in two coupled climate models, Deep Sea Res. Part II Top. Stud.
600 Oceanogr., 61–64, 114–126, doi:10.1016/j.dsr2.2011.12.002, 2012.

601 Dansgaard, W., Johnsen, S. J., Clausen, H. B., Dahl-Jensen, D., Gundestrup, N. S., Hammer, C. U.,
602 Hvidberg, C. S., Steffensen, J. P., Sveinbjörn, Jouzel, J. and Bond, G. C.: Evidence for general
603 instability of past climate from a 250-kyr ice-core record, Nature, 364(6434), 218–220,
604 doi:10.1038/364218a0, 1993.

605 Dykoski, C. A., Edwards, R. L., Cheng, H., Yuan, D., Cai, Y., Zhang, M., Lin, Y., Qing, J., An, Z.
606 and Revenaugh, J.: A high-resolution, absolute-dated Holocene and deglacial Asian monsoon
607 record from Dongge Cave, China, Earth Planet. Sci. Lett., 233(1–2), 71–86,
608 doi:10.1016/j.epsl.2005.01.036, 2005.

609 Dymond, J., Suess, E. and Lyle, M.: Barium in Deep-Sea Sediment: A Geochemical Proxy for
610 Paleoproductivity, Paleoceanography, 7(2), 163–181, doi:10.1029/92PA00181, 1992.

611 Enkin, R. J., Baker, J., Nourgaliev, D., Iassonov, P. and Hamilton, T. S.: Magnetic hysteresis
612 parameters and Day plot analysis to characterize diagenetic alteration in gas hydrate-bearing
613 sediments, J. Geophys. Res., 112(B06S90), 1–13, doi:10.1029/2006JB004638, 2007.

614 EPICA Community Members: One-to-one coupling of glacial climate variability in Greenland and
615 Antarctica, Nature, 444(7116), 195–198, doi:10.1038/nature05301, 2006.

616 Favorite, F., Dodimead, A. J. and Nasu, K.: Oceanography of the Subarctic Pacific region, 1960-
617 1971., 1976.

618 Fletcher, W. J., Sanchez Goñi, M. F., Allen, J. R. M., Cheddadi, R., Combourieu-Nebout, N.,
619 Huntley, B., Lawson, I., Londeix, L., Magri, D., Margari, V., Müller, U. C., Naughton, F.,
620 Novenko, E., Roucoux, K. and Tzedakis, P. C.: Millennial-scale variability during the last glacial in
621 vegetation records from Europe, Quat. Sci. Rev., 29(21–22), 2839–2864,
622 doi:10.1016/j.quascirev.2009.11.015, 2010.

623 Galbraith, E. D., Jaccard, S. L., Pedersen, T. F., Sigman, D. M., Haug, G. H., Cook, M., Southon, J.
624 R. and Francois, R.: Carbon dioxide release from the North Pacific abyss during the last
625 deglaciation., Nature, 449(7164), 890–893, doi:10.1038/nature06227, 2007.

626 Gebhardt, H., Sarnthein, M., Grootes, P. M., Kiefer, T., Kuehn, H., Schmieder, F. and Röhl, U.:
627 Paleonutrient and productivity records from the subarctic North Pacific for Pleistocene glacial
628 terminations I to V, Paleoceanography, 23(4), doi:10.1029/2007PA001513, 2008.

629 Goldberg, E. D. and Arrhenius, G. O. S.: Chemistry of Pacific pelagic sediments, Geochim.

630 Cosmochim. Acta, 13(2–3), 153–212, doi:10.1016/0016-7037(58)90046-2, 1958.

631 Goldberg, E. L. E. L., Gorbarenko, S. A. S. A., Shaporenko, A. D., Bosin, A. A. A. A., Leskov, V.

632 Y. Y. and Chebykin, E. P. P.: Instability of last glacial climate from SRXFA data for bottom

633 sediments in the Okhotsk Sea, Nucl. Instruments Methods Phys. Res. Sect. A Accel. Spectrometers,

634 Detect. Assoc. Equip., 543(1), 284–287, doi:10.1016/j.nima.2005.01.242, 2005.

635 Gorbarenko, S. A.: Stable Isotope and Lithologic Evidence of Late-Glacial and Holocene

636 Oceanography of the Northwestern Pacific and Its Marginal Seas, Quat. Res., 46(3), 230–250,

637 doi:10.1006/qres.1996.0063, 1996.

638 Gorbarenko, S. A. and Goldberg, E. L.: Assessment of Variations of Primary Production in the Sea

639 of Okhotsk, Bering Sea, and Northwestern Pacific over the Last Glaciation Maximum and

640 Holocene, Dokl. Earth Sci., 405(9), 1380–1383, 2005.

641 Gorbarenko, S. A., Chekhovskaya, M. P. and Southon, J. R.: Detailed environmental changes of the

642 Okhotsk Sea central part during last Glaciation Holocene, Oceanologia, 38(2), 305–308, 1998.

643 Gorbarenko, S. A., Leskov, V. Y., Artemova, A. V., Tiedemann, R., Biebow, N. and Nürnberg, D.:

644 Ice Cover of the Sea of Okhotsk during the Last Glaciation and Holocene, Dokl. Earth Sci., 389(2),

645 208–211, 2003.

646 Gorbarenko, S. A., Southon, J. R. J. ., Keigwin, L. D., Cherepanova, M. . and Gvozdeva, I. . G.:

647 Late Pleistocene–Holocene oceanographic variability in the Okhotsk Sea: geochemical, lithological

648 and paleontological evidence, Palaeogeogr. Palaeoclimatol. Palaeoecol., 209(1–4), 281–301,

649 doi:10.1016/j.palaeo.2004.02.013, 2004.

650 Gorbarenko, S. A., Basov, I. A., Chekhovskaya, M. P. P., Southon, J. R., Khusid, T. A. A. and

651 Artemova, A. V.: Orbital and millennium scale environmental changes in the southern Bering Sea

652 during the last glacial-Holocene: Geochemical and paleontological evidence, Deep Sea Res. Part II

653 Top. Stud. Oceanogr., 52(16–18), 2174–2185, doi:10.1016/j.dsr2.2005.08.005, 2005.

654 Gorbarenko, S. A. S. A., Harada, N., Malakhov, M. I. M. I., Velivetskaya, T. A. T. A., Vasilenko,

655 Y. P. Y. P., Bosin, A. A. A. A., Derkachev, A. N. A. N., Goldberg, E. L. E. L. and Ignatiev, A. V.

656 A. V.: Responses of the Okhotsk Sea environment and sedimentology to global climate changes at

657 the orbital and millennial scale during the last 350kyr, Deep Sea Res. Part II Top. Stud. Oceanogr.,

658 61–64, 73–84, doi:10.1016/j.dsr2.2011.05.016, 2012.

659 Harada, N.: MIRAI cruise report MR06-04 Leg 1 and 2, JAMSTEC, Yokosuka. [Available at

660 http://www.godac.jamstec.go.jp/cruisedata/mirai/e/MR06-04_leg1.html]., 2006.

661   Harada, N., Sato, M. and Sakamoto, T.: Freshwater impacts recorded in tetraunsaturated alkenones
662   and alkenone sea surface temperatures from the Okhotsk Sea across millennial-scale cycles,
663   Paleoceanography, 23(3), doi:10.1029/2006PA001410, 2008.

664   Harris, P. G., Zhao, M., Rosell-Melé, A., Tiedemann, R., Sarnthein, M. and Maxwell, J. R.: Chlorin
665   accumulation rate as a proxy for Quaternary marine primary productivity, Nature, 383(6595), 63–
666   65, doi:10.1038/383063a0, 1996.

667   Hong, Y. T., Hong, B., Lin, Q. H., Shibata, Y., Zhu, Y. X., Leng, X. T. and Wang, Y.: Synchronous
668   climate anomalies in the western North Pacific and North Atlantic regions during the last 14,000
669   years, Quat. Sci. Rev., 28(9–10), 840–849, doi:10.1016/j.quascirev.2008.11.011, 2009.

670   Hu, F. S., Kaufman, D., Yoneji, S., Nelson, D., Shemesh, A., Huang, Y., Tian, J., Bond, G. C.,
671   Clegg, B. and Brown, T. A.: Cyclic variation and solar forcing of Holocene climate in the Alaskan
672   subarctic., Science, 301(5641), 1890–1893, doi:10.1126/science.1088568, 2003.

673   Jaccard, S. L., Galbraith, E. D., Sigman, D. M. and Haug, G. H.: A pervasive link between
674   Antarctic ice core and subarctic Pacific sediment records over the past 800 kyrs, Quat. Sci. Rev.,
675   29(1–2), 206–212, doi:10.1016/j.quascirev.2009.10.007, 2010.

676   Jasonov, P. G., Nurgaliev, D. K., Burov, B. V. and Heller, F.: A modernized coercivity
677   spectrometer, Geol. Carpathica, 49(3), 2254–225, 1998.

678   Jin, L., Chen, F., Ganopolski, A. and Claussen, M.: Response of East Asian climate to
679   Dansgaard/Oeschger and Heinrich events in a coupled model of intermediate complexity, J.
680   Geophys. Res., 112(D6), D06117, doi:10.1029/2006JD007316, 2007.

681   Johnsen, S. J., Clausen, H. B., Dansgaard, W., Fuhrer, K., Gundestrup, N., Hammer, C. U., Iversen,
682   P., Jouzel, J., Stauffer, B. and Steffensen, J. P.: Irregular glacial interstadials recorded in a new
683   Greenland ice core, Nature, 359(6393), 311–313, doi:10.1038/359311a0, 1992.

684   Keigwin, L. D.: Glacial-age hydrography of the far northwest Pacific Ocean, Paleoceanography,
685   13(4), 323–339, doi:10.1029/98PA00874, 1998.

686   Keigwin, L. D., Jones, G. A. and Froelich, P. N.: A 15,000 year paleoenvironmental record from
687   Meiji Seamount, far northwestern Pacific, Earth Planet. Sci. Lett., 111(2–4), 425–440,
688   doi:10.1016/0012-821X(92)90194-Z, 1992.

689   Kennett, J. P., Roark, E. B., Cannariato, K. G., Ingram, B. L. and Tada, R.: Latest quaternary
690   paleoclimatic and radiocarbon chronology, Hole 1017E, Southern California margin, Proc. Ocean
691   Drill. Progr., 167, 249–254, 2000.

692 Kiefer, T., Sarnthein, M., Erlenkeuser, H., Grootes, P. M. and Roberts, A. P.: North Pacific
693 response to millennial-scale changes in ocean circulation over the last 60 kyr, Paleoceanography,
694 16(2), 179–189, doi:10.1029/2000PA000545, 2001.

695 Kienast, S. S. and McKay, J. L.: Sea surface temperature in the subartic Northeast Pacific reflect
696 millennial-scale climate oscillations during the last 16 kyr, Geophys. Res. Lett., 28(8), 1563–1566,
697 2001.

698 Kim, S.-J., Khim, B.-K., Uchida, M., Itaki, T. and Tada, R.: Millennial-scale paleoceanographic
699 events and implication for the intermediate-water ventilation in the northern slope area of the
700 Bering Sea during the last 71 kyrs, Glob. Planet. Change, 79(1–2), 89–98,
701 doi:10.1016/j.gloplacha.2011.08.004, 2011.

702 Kimura, N. and Wakatsuchi, M.: Processes controlling the advance and retreat of sea ice in the Sea
703 of Okhotsk, J. Geophys. Res., 104(C5), 11137, doi:10.1029/1999JC900004, 1999.

704 Lisitzin, A. P.: Sea-Ice and Iceberg Sedimentation in the Ocean, Springer, Berlin, Heidelberg.,
705 2002.

706 Malakhov, M. I. M. I., Gorbarenko, S. A. S. A., Malakhova, G. Y., Harada, N., Vasilenko, Y. P.,
707 Bosin, A. A. A. A., Gol'dberg, E. L., Derkachev, A. N. A. N., Goldberg, E. L. and Derkachev, A.
708 N. A. N.: Petromagnetic parameters of bottom sediments as indicators of the climatic and
709 environmental changes in the central zone of the Sea of Okhotsk during the last 350 kyr, Russ.
710 Geol. Geophys., 50(11), 973–982, doi:10.1016/j.rgg.2009.10.006, 2009.

711 Max, L., Riethdorf, J.-R., Tiedemann, R., Smirnova, M., Lembke-Jene, L., Fahl, K., Nürnberg, D.,
712 Matul, A. G. and Mollenhauer, G.: Sea surface temperature variability and sea-ice extent in the
713 subarctic northwest Pacific during the past 15,000 years, Paleoceanography, 27(3),
714 doi:10.1029/2012PA002292, 2012.

715 Max, L., Lembke-Jene, L., Riethdorf, J.-R., Tiedemann, R., Nürnberg, D., Kühn, H. and
716 Mackensen, A.: Pulses of enhanced North Pacific Intermediate Water ventilation from the Okhotsk
717 Sea and Bering Sea during the last deglaciation, Clim. Past, 10(2), 591–605, doi:10.5194/cp-10-
718 591-2014, 2014.

719 McManus, J., Berelson, W. M., Klinkhammer, G. P., Johnson, K. S., Coale, K. H., Anderson, R. F.,
720 Kumar, N., Burdige, D. J., Hammond, D. E., Brumsack, H. J., McCorkle, D. C. and Rushdi, A.:
721 Geochemistry of barium in marine sediments: implications for its use as a paleoproxy, Geochim.
722 Cosmochim. Acta, 62(21–22), 3453–3473, doi:10.1016/S0016-7037(98)00248-8, 1998.

723 McManus, J. F., Francois, R., Gherardi, J.-M., Keigwin, L. D. and Brown-Leger, S.: Collapse and

rapid resumption of Atlantic meridional circulation linked to deglacial climate changes., Nature, 428(6985), 834–837, doi:10.1038/nature02494, 2004.

Nagashima, K., Tada, R., Tani, A., Sun, Y., Isozaki, Y., Toyoda, S. and Hasegawa, H.: Millennial-scale oscillations of the westerly jet path during the last glacial period, J. Asian Earth Sci., 40(6), 1214–1220, doi:10.1016/j.jseaes.2010.08.010, 2011.

Narita, H., Sato, M., Tsunogai, S., Murayama, M., Ikehara, M., Nakatsuka, T., Wakatsuchi, M., Harada, N. and Ujiié, Y.: Biogenic opal indicating less productive northwestern North Pacific during the glacial ages, Geophys. Res. Lett., 29(15), 22-1-22–4, doi:10.1029/2001GL014320, 2002.

Nilsson, T.: The Pleistocene; Geology and Life in the Quaternary Ice Age, D. Reidel, Dordrecht., 1983.

North Greenland Ice Core Project members: High-resolution record of Northern Hemisphere climate extending into the last interglacial period, Nature, 431(7005), 147–151, doi:10.1038/nature02805, 2004.

Nürnberg, D. and Tiedemann, R.: Environmental change in the Sea of Okhotsk during the last 1.1 million years, Paleoceanography, 19(4), PA4011, doi:10.1029/2004PA001023, 2004.

Okazaki, Y., Timmermann, A., Menviel, L., Harada, N., Abe-Ouchi, A., Chikamoto, M. O., Mouchet, A. and Asahi, H.: Deepwater formation in the North Pacific during the Last Glacial Termination., Science, 329(5988), 200–204, doi:10.1126/science.1190612, 2010.

Praetorius, S. K. and Mix, A. C.: Synchronization of North Pacific and Greenland climates preceded abrupt deglacial warming, Science, 345(6195), 444–448, doi:10.1126/science.1252000, 2014.

Prahl, F. G., Muehlhausen, L. A. and Lyle, M.: An organic geochemical assessment of oceanographic conditions at Manop Site C over the past 26,000 years, Paleoceanography, 4(5), 495–510, doi:10.1029/PA004i005p00495, 1989.

Rasmussen, S. O., Bigler, M., Blockley, S. P., Blunier, T., Buchardt, S. L., Clausen, H. B., Cvijanovic, I., Dahl-Jensen, D., Johnsen, S. J., Fischer, H., Gkinis, V., Guillevic, M., Hoek, W. Z., Lowe, J. J., Pedro, J. B., Popp, T., Seierstad, I. K., Steffensen, J. P., Svensson, A. M., Vallelonga, P., Vinther, B. M., Walker, M. J. C., Wheatley, J. J. and Winstrup, M.: A stratigraphic framework for abrupt climatic changes during the Last Glacial period based on three synchronized Greenland ice-core records: refining and extending the INTIMATE event stratigraphy, Quat. Sci. Rev., 106, 14–28, doi:10.1016/j.quascirev.2014.09.007, 2014.

Reimer, P. J., Baillie, M. G. L., Bard, E., Beck, J. W., Bertrand, C. J. H., Blackwell, P. G., Buck, C.

E., Burr, G. S., Cutler, K. B., Damon, P. E., Edwards, R. L., Fairbanks, R. G., Friedrich, M. and Guilderson, T. P.: IntCal04 terrestrial radiocarbon age calibration, 0–26 cal kyr BP, Radiocarbon, 46(3), 1029–1058, 2004.

Reimer, P. J., Bard, E., Bayliss, A., Beck, J. W., Blackwell, P. G., Bronk Ramsey, C., Buck, C. E., Cheng, H., Edwards, R. L., Friedrich, M., Grootes, P. M., Guilderson, T. P., Haflidason, H., Hajdas, I., Hatte, C., Heaton, T. J., Hoffmann, D. L., Hogg, A. G., Hughen, K. A., Kaiser, K. F., Kromer, B., Manning, S. W., Niu, M., Reimer, R. W., Richards, D. A., Scott, E. M., Southon, J. R., Staff, R. A., Turney, C. S. M. and van der Plicht, J.: IntCal13 and Marine13 Radiocarbon Age Calibration Curves 0–50,000 Years cal BP, Radiocarbon, 55(4), 1869–1887, doi:10.2458/azu_js_rc.55.16947, 2013.

Riethdorf, J.-R., Nürnberg, D., Max, L., Tiedemann, R., Gorbarenko, S. A. and Malakhov, M. I.: Millennial-scale variability of marine productivity and terrigenous matter supply in the western Bering Sea over the past 180 kyr, Clim. Past, 9(3), 1345–1373, doi:10.5194/cp-9-1345-2013, 2013.

Riethdorf, J.-R., Thibodeau, B., Ikehara, M., Nürnberg, D., Max, L., Tiedemann, R., Yokoyama, Y., Riethdorf, J.-R., Thibodeau, B., Ikehara, M., Nürnberg, D., Max, L., Tiedemann, R. and Yokoyama, Y.: Surface nitrate utilization in the Bering sea since 180kA BP: Insight from sedimentary nitrogen isotopes, Deep Sea Res. Part II Top. Stud. Oceanogr., 125–126, 163–176, doi:10.1016/j.dsr2.2015.03.007, 2016.

Röhl, U. and Abrams, L. J.: High-resolution, downhole, and nondestructive core measurements from Sites 999 and 1001 in the Caribbean Sea: application to the Late Paleocene Thermal Maximum, in Proceedings of the Ocean Drilling Program, 165 Scientific Results, vol. 165, pp. 191–203, Ocean Drilling Program., 2000.

Rohling, E. J., Liu, Q. S., Roberts, a. P., Stanford, J. D., Rasmussen, S. O., Langen, P. L. and Siddall, M.: Controls on the East Asian monsoon during the last glacial cycle, based on comparison between Hulu Cave and polar ice-core records, Quat. Sci. Rev., 28, 3291–3302, doi:10.1016/j.quascirev.2009.09.007, 2009.

Rossignol-Strick, M.: Mediterranean Quaternary sapropels, an immediate response of the African monsoon to variation of insolation, Palaeogeogr. Palaeoclimatol. Palaeoecol., 49(3–4), 237–263, doi:10.1016/0031-0182(85)90056-2, 1985.

Rothwell, R. G.: The Smear Slide Method, in Minerals and Mineraloids in Marine Sediments, pp. 21–24, Springer Netherlands, Dordrecht., 1989.

Ruth, U., Bigler, M., Röthlisberger, R., Siggaard-Andersen, M.-L., Kipfstuhl, S., Goto-Azuma, K.,

787 Hansson, M. E., Johnsen, S. J., Lu, H. and Steffensen, J. P.: Ice core evidence for a very tight link
788 between North Atlantic and east Asian glacial climate, Geophys. Res. Lett., 34(L03706), 1–5,
789 doi:10.1029/2006GL027876, 2007.

790 Sakamoto, T., Ikehara, M., Aoki, K., Iijima, K., Kimura, N., Nakatsuka, T. and Wakatsuchi, M.:
791 Ice-rafted debris (IRD)-based sea-ice expansion events during the past 100 kyrs in the Okhotsk Sea,
792 Deep Sea Res. Part II Top. Stud. Oceanogr., 52(16–18), 2275–2301,
793 doi:10.1016/j.dsr2.2005.08.007, 2005.

794 Sarnthein, M., Kiefer, T., Grootes, P. M., Elderfield, H. and Erlenkeuser, H.: Warmings in the far
795 northwestern Pacific promoted pre-Clovis immigration to America during Heinrich event 1,
796 Geology, 34(3), 141–144, doi:10.1130/G22200.1, 2006.

797 Schlung, S. A., Christina Ravelo, A., Aiello, I. W., Andreasen, D. H., Cook, M. S., Drake, M.,
798 Dyez, K. A., Guilderson, T. P., LaRiviere, J. P., Stroynowski, Z. and Takahashi, K.: Millennial-
799 scale climate change and intermediate water circulation in the Bering Sea from 90 ka: A high-
800 resolution record from IODP Site U1340, Paleoceanography, 28(1), 54–67,
801 doi:10.1029/2012PA002365, 2013.

802 Seierstad, I. K., Abbott, P. M., Bigler, M., Blunier, T., Bourne, A. J., Brook, E. J., Buchardt, S. L.,
803 Buizert, C., Clausen, H. B., Cook, E., Dahl-Jensen, D., Davies, S. M., Guillevic, M., Johnsen, S. J.,
804 Pedersen, D. S., Popp, T. J., Rasmussen, S. O., Severinghaus, J. P., Svensson, A. and Vinther, B.
805 M.: Consistently dated records from the Greenland GRIP, GISP2 and NGRIP ice cores for the past
806 104 ka reveal regional millennial-scale δ18O gradients with possible Heinrich event imprint, Quat.
807 Sci. Rev., 106, 29–46, doi:10.1016/j.quascirev.2014.10.032, 2014.

808 Seki, O., Ishiwatari, R. and Matsumoto, K.: Millennial climate oscillations in NE Pacific surface
809 waters over the last 82 kyr: New evidence from alkenones, Geophys. Res. Lett., 29(23), 59-1-59–4,
810 doi:10.1029/2002GL015200, 2002.

811 Seki, O., Ikehara, M., Kawamura, K., Nakatsuka, T., Ohnishi, K., Wakatsuchi, M., Narita, H. and
812 Sakamoto, T.: Reconstruction of paleoproductivity in the Sea of Okhotsk over the last 30 kyr,
813 Paleoceanography, 19(1), doi:10.1029/2002PA000808, 2004.

814 Serno, S., Winckler, G., Anderson, R. F., Maier, E., Ren, H., Gersonde, R. and Haug, G. H.:
815 Comparing dust flux records from the Subarctic North Pacific and Greenland: Implications for
816 atmospheric transport to Greenland and for the application of dust as a chronostratigraphic tool,
817 Paleoceanography, 30(6), 583–600, doi:10.1002/2014PA002748, 2015.

818 Siddall, M., Kaplan, M. R., Schaefer, J. M., Putnam, A., Kelly, M. A. and Goehring, B.: Changing

819   influence of Antarctic and Greenlandic temperature records on sea-level over the last glacial cycle,

820   Quat. Sci. Rev., 29(3–4), 410–423, doi:10.1016/j.quascirev.2009.11.007, 2010.

821   Stuiver, M. and Reimer, P. J.: Extended 14C Data Base and Revised Calib 3.0 14C Age Calibration

822   Program, Radiocarbon, 35(1), 215–230, 1993.

823   Stuiver, M., Grootes, P. M. and Braziunas, T. F.: The GISP2 δ18O Climate Record of the Past

824   16,500 Years and the Role of the Sun, Ocean, and Volcanoes, Quat. Res., 44(3), 341–354,

825   doi:10.1006/qres.1995.1079, 1995.

826   Sun, Y., Clemens, S. C., Morrill, C., Lin, X., Wang, X. and An, Z.: Influence of Atlantic meridional

827   overturning circulation on the East Asian winter monsoon, Nat. Geosci., 5(1), 46–49,

828   doi:10.1038/ngeo1326, 2012.

829   Sung, M.-K., Kwon, W.-T., Baek, H.-J., Boo, K.-O., Lim, G.-H. and Kug, J.-S.: A possible impact

830   of the North Atlantic Oscillation on the east Asian summer monsoon precipitation, Geophys. Res.

831   Lett., 33(21), L21713, doi:10.1029/2006GL027253, 2006.

832   Tarasov, P. E., Bezrukova, E. V. and Krivonogov, S. K.: Late Glacial and Holocene changes in

833   vegetation cover and climate in southern Siberia derived from a 15 kyr long pollen record from

834   Lake Kotokel, Clim. Past, 5(3), 285–295, doi:10.5194/cp-5-285-2009, 2009.

835   Tauxe, L.: Sedimentary records of relative paleointenstiy of the geomagnetic field: theory and

836   practice, Rev. Geophys., 31(93), 319–354, 1993.

837   Timmermann, A., Lorenz, S. J., An, S.-I., Clement, A. and Xie, S.-P.: The Effect of Orbital Forcing

838   on the Mean Climate and Variability of the Tropical Pacific, J. Clim., 20(16), 4147–4159,

839   doi:10.1175/JCLI4240.1, 2007.

840   Walker, M. J. C., Berkelhammer, M., Björck, S., Cwynar, L. C., Fisher, D. A., Long, A. J., Lowe, J.

841   J., Newnham, R. M., Rasmussen, S. O. and Weiss, H.: Formal subdivision of the Holocene

842   Series/Epoch: a Discussion Paper by a Working Group of INTIMATE (Integration of ice-core,

843   marine and terrestrial records) and the Subcommission on Quaternary Stratigraphy (International

844   Commission on Stratigraphy), J. Quat. Sci., 27(7), 649–659, doi:10.1002/jqs.2565, 2012.

845   Wang, Y., Cheng, H., Edwards, R. L., An, Z., Wu, J., Shen, C.-C. and Dorale, J. A.: A high-

846   resolution absolute-dated late Pleistocene Monsoon record from Hulu Cave, China., Science,

847   294(5550), 2345–8, doi:10.1126/science.1064618, 2001.

848   Wang, Y., Cheng, H., Edwards, R. L., He, Y., Kong, X., An, Z., Wu, J., Kelly, M. J., Dykoski, C.

849   A. and Li, X.: The Holocene Asian monsoon: links to solar changes and North Atlantic climate.,

850   Science, 308(5723), 854–857, doi:10.1126/science.1106296, 2005.

851   Wang, Y., Cheng, H., Edwards, R. L., Kong, X., Shao, X., Chen, S., Wu, J., Jiang, X., Wang, X.

852   and An, Z.: Millennial- and orbital-scale changes in the East Asian monsoon over the past 224,000

853   years., Nature, 451(7182), 1090–1093, doi:10.1038/nature06692, 2008.

854   Wu, B. and Wang, J.: Winter Arctic Oscillation, Siberian High and East Asian Winter Monsoon,

855   Geophys. Res. Lett., 29(19), 3-1-3–4, doi:10.1029/2002GL015373, 2002.

856   Xue, F., Wang, H. and He, J.: Interannual Variability of Mascarene High and Australian High and

857   Their Influences on East Asian Summer Monsoon, J. Meteorol. Soc. Japan, 82(4), 1173–1186,

858   doi:10.2151/jmsj.2004.1173, 2004.

859   Yu, J., Anderson, R. F., Jin, Z., Rae, J. W. B., Opdyke, B. N. and Eggins, S. M.: Responses of the

860   deep ocean carbonate system to carbon reorganization during the Last Glacial–interglacial cycle,

861   Quat. Sci. Rev., 76, 39–52, doi:10.1016/j.quascirev.2013.06.020, 2013.

862   Yu, Y., Yang, T., Li, J., Liu, J., An, C., Liu, X., Fan, Z., Lu, Z., Li, Y. and Su, X.: Millennial-scale

863   Holocene climate variability in the NW China drylands and links to the tropical Pacific and the

864   North Atlantic, Palaeogeogr. Palaeoclimatol. Palaeoecol., 233(1–2), 149–162,

865   doi:10.1016/j.palaeo.2005.09.008, 2006.

866   Yuan, D., Cheng, H., Edwards, R. L., Dykoski, C. A., Kelly, M. J., Zhang, M., Qing, J., Lin, Y.,

867   Wang, Y., Wu, J., Dorale, J. A., An, Z. and Cai, Y.: Timing, duration, and transitions of the last

868   interglacial Asian monsoon., Science, 304(5670), 575–578, doi:10.1126/science.1091220, 2004.

869   Zijderveld, J. D. A.: A. C. demagnetization of rocks : analysis of results, in Methods in

870   Palaeomagnetism, edited by D. W. Collinson, K. M. Creer, and S. K. Runcorn, pp. 254–286,

871   Elsevier., 1964.

872

873

Captions

Table 1. AMS ^{14}C data in monospecies planktic foraminifera *N. pachyderma* sin. and benthic
foraminifera *Epistominella pacifica* and *Uvigerina parvocostata* of core 41-2. All measured AMS
[14]C data were calibrated by Calib 6.0 (Stuiver and Reimer, 1993) with Marine13 calibration curve
(Reimer et al., 2013) with a surface water reservoir ages of 900 years (Max et al., 2014). In case of
using benthic foraminifera for dating, we accept difference in paired benthic-planktic foraminifera
ages equals to 1,400 years, based on unpublished data and total regional results of Max et al.
(2014). All radiocarbon ages were converted into calibrated 1-sigma calendar age.

#	Lab. code	core depth cm	foraminifera species	14C-age year	Err.1 sigma year	calendar age, ka
1	YAUT-021713	120	*E. pacifica*	10078	47	9.121
2	YAUT-021714	127.5	*E. pacifica*	10340	42	9.445
3	UCIAMS-148095	298	*N. pachyd.*	13160	50	14.393
4	UCIAMS-148096	156	*Uv. parvoc.*	11135	45	10.60
5	UCIAMS-148098	306	*Uv. parvoc.*	14185	35	14.616

884   Table 2. Centennial events with increased / decreased productivity during 25-8 ka in core 41-2 and

885   the average ages according to the correlations between productivity events and the EASM sub-

886   interstadials and sub-stadials (CsI/CsS).

887

Events	Core interval, cm	Averaged cal. age, ka
CsS-EH-1	105-110	8.2
CsI-EH-1	111-116	8.6
CsS-EH-2	117-123	9.1
CsI-EH-2	124-129	9.5
CsS-EH-3	131-140	9.9
CsI-EH-3	141-153	10.5
CsS-EH-4	155-167	11.1
CsI-EH-4	168-181	11.5
CsI-GI1-a	231-238	13.1
CsI-GI1-c1	248-262	13.5
CsI-GI1-c3	269-279	13.8
CsI-GI1-e	285-306	14.3
CsI-GS2.1-1	317-322	14.9
CsI-GS2.1-2	335-339	15.5
CsI-GS2.1-3	353-360	16.5
CsI-GS2.1-4	373-381	17.5
CsI-GS2.1-5	388-395	18.1
CsI-GS2.1-6	399-407	18.6
CsI-GS2.1-7	420-425	19.2
CsI-GS2.1-8	432-437	19.5

888

889

890

891 Table 3. The age controlling points of core 41-2 is derived from available AMS ^{14}C data of core 41-
892 2, projection AMS 14C age of core 12KL, and tie points through correlation between increased
893 productivity events and EASM CsIs (Wang et al., 2008). One AMS ^{14}C datum of core 12KL at
894 depth of 706 cm was accepted according to the Tiedemann/Max age model 2 (Max et al., 2012,
895 2014).

896

| Depth	AMS 14C core 41-2	Key time points of core 12KL	correlation with ages of China subInterstadial	Accepted key time points
cm	Cal. age, ka	ka/ depth (cm)		Cal. age, ka
120	9.12			9.12
127.5	9.45			
126		9.51/210		9.51
156	10.6			
159		11.08/295		11.08
167		11.31/340		11.31
234			13.08/GsI-GI1-a	13.08
251		13.42/508		13.42
273		13.79/550		13.79
298	14.39			
303		14.42/611		14.42
306	14.61			
337			15.42/CsI-GS2.1-2	15.42
348		16.16/706		16.16
357			16.51/ CsI-GS2.1-3	16.51
379			17.56/ CsI-GS2.1-4	17.56
393			18.12/ CsI-GS2.1-5	18.12
402		18.6/821		18.6
405			18.78/ CsI-GS2.1-6	18.78
423			19.25/ CsI-GS2.1-7	19.25
434		19.54/876		19.54

897

898

899
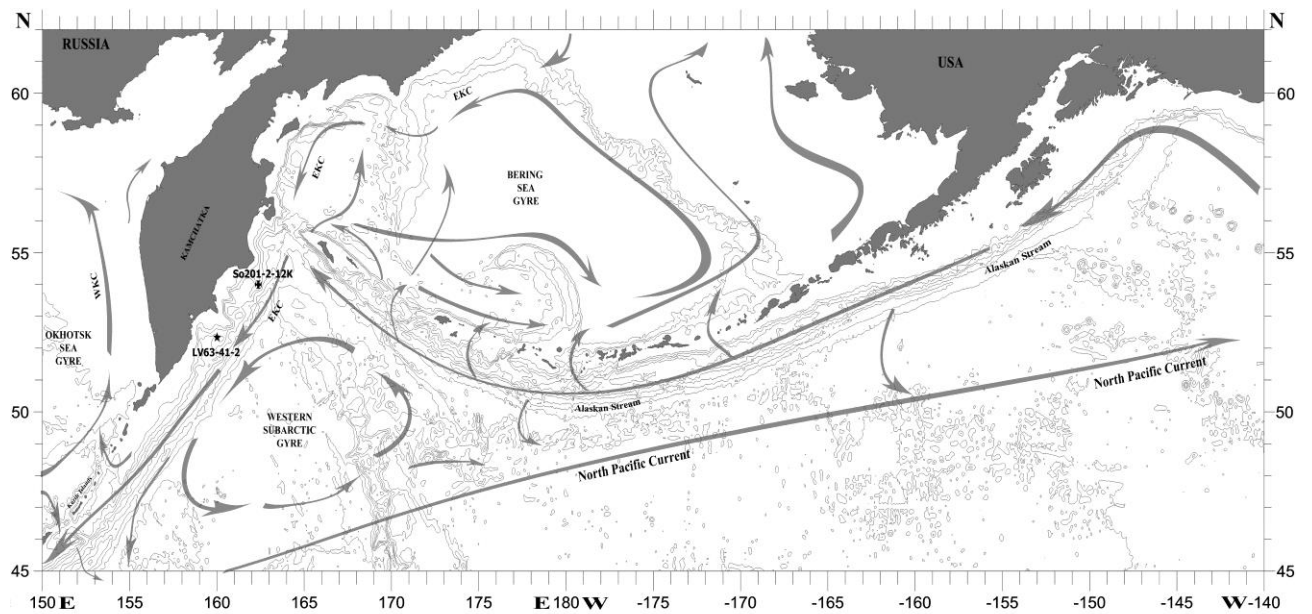
Fig. 1. Bathymetry, surface water currents and location of the cores 41-2 (star) and 12KL (cross) (Max et al., 2012) in the N Pacific. Surface currents as in (Favorite et al., 1976) with modifications. EKC – East Kamchatka Current, WKC – West Kamchatka Current.
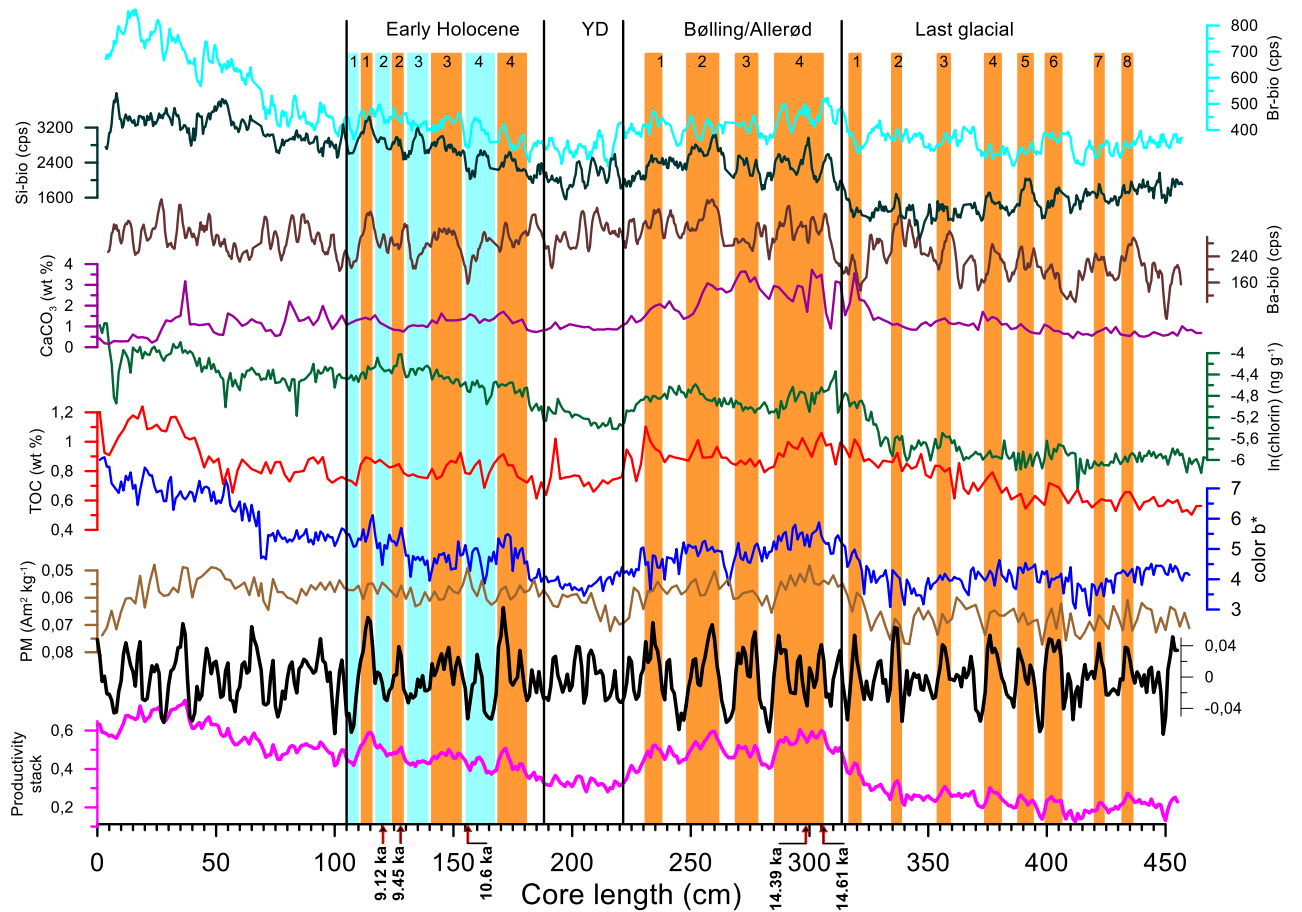
Fig. 2. Records (from bottom to top) of the original and detrended productivity stacks, PM, color b*, TOC, chlorin, CaCO₃, Ba-bio, Si-bio, and Br-bio versus depth. Preliminary boundaries of the B/A warming, YD cooling, and Holocene are shown according to general variability of productivity in the NW Pacific, Sea of Okhotsk, and Bering Sea (Galbraith et al., 2007; Gorbarenko, 1996; Gorbarenko and Goldberg, 2005; Keigwin, 1998; Seki et al., 2004). AMS ^{14}C data (calendar ka) were shown at the base. Blue bars indicate cold periods / lower productivity events. Orange bars indicate warm periods / high producitivity events.
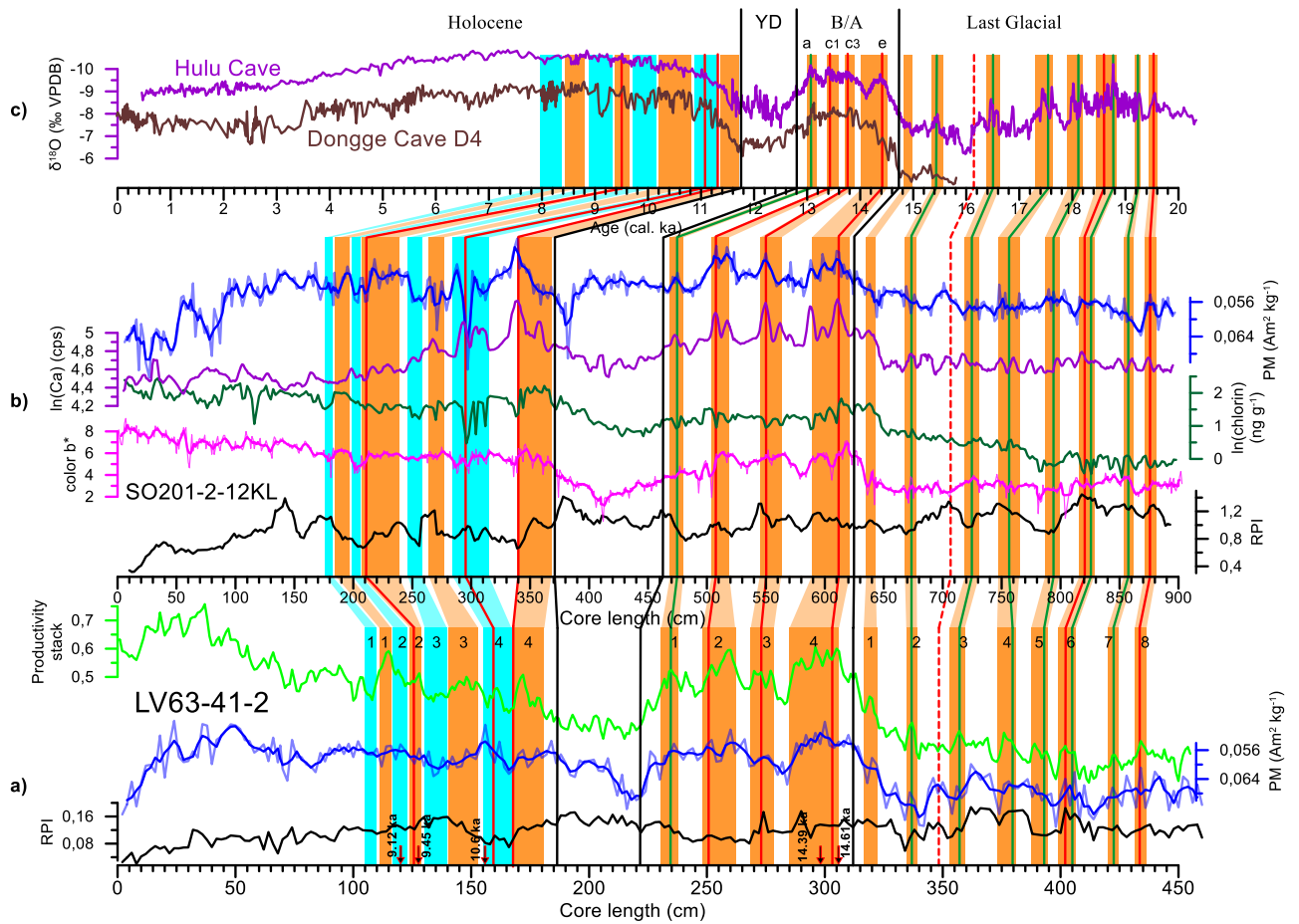
Fig. 3. Age model of core 41-2. Low panel: (a) RPI, PM and productivity stack of core 41-2 versus depth. (b) Middle panel: RPI, color b*, chlorin, Ca and PM of core 12KL versus depth. (c) Upper panel: δ¹⁸O calcite of Chinese cave stalagmites (Dykoski et al., 2005; Wang et al., 2008) over the last 20 ka. The correlation of productivity events between core 41-2 and 12KL was established according to correlation of productivity stack of core 41-2 with productivity proxies of core 12KL and the RPI records of both cores. AMS ¹⁴C data of core 12KL (red lines) were projected to the core 41-2 according to correlated productivity events. A close correlation of the productivity events with sub-interstadials in the EASM becomes apparent after projection of the radiocarbon data on the age scale of EASM. Green lines correlate EASM sub-interstadials with productivity events. Orange and blue bars are as in Fig. 2.
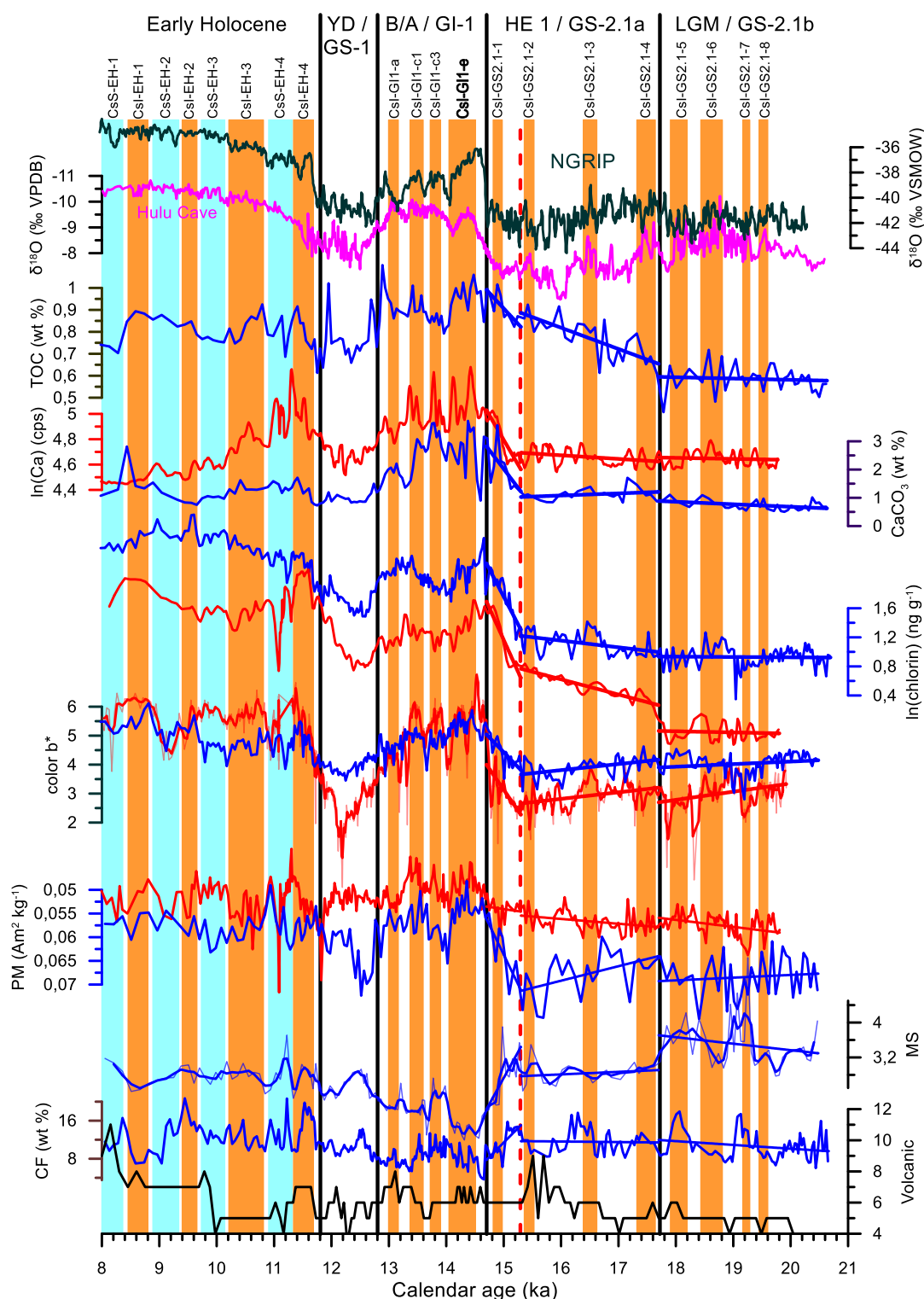
Fig. 4. High resolution variability of the productivity and lithologic proxies in the NW Pacific during 21–8 ka. Volcanic particles, CF, MS, PM, color b*, chlorin, CaCO₃/Ca, and TOC determined in cores 41-2 (blue lines) and 12KL (red lines) are shown from bottom to top. Δ18O records of EASM (Wang et al., 2008) and NGRIP (North Greenland Ice Core Project members, 2004) are shown at the top of the figure. Linear trends are shown for productivity and lithologic proxies during 20-17.8, 17.8-15.3, and 15.3-14.7 ka periods. Red dashed line marks the boundary in productivity and lithologic trends during HE1 at 15.3 kyr. Orange and blue bars are as in Fig. 2.
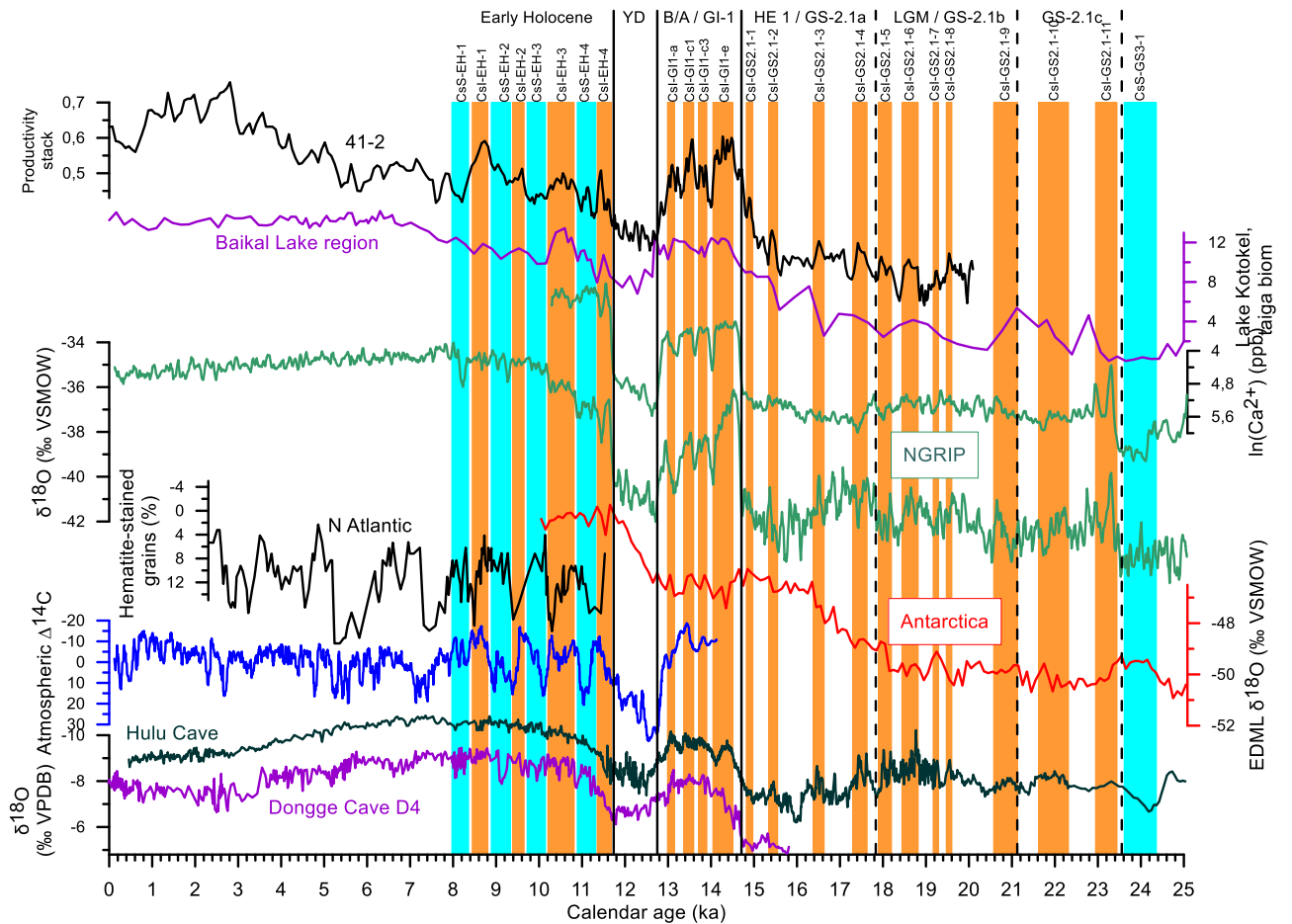
935
936 Fig. 5. Compilations of Northern and Southern Hemisphere climate records, solar activity, NW
937 Pacific productivity events, and vegetation records from the southern Siberia during the last 25 ka.
938 From bottom to top: absolutely dated $\delta^{18}O$ calcite of Chinese cave stalagmites (Dykoski et al., 2005;
939 Wang et al., 2008); the residual atmospheric $\Delta^{14}C$ record of around 2000-year moving average
940 (Reimer et al., 2004); $\delta^{18}O$ EDML records after methane synchronization with the N Greenland ice
941 core (EPICA Community Members, 2006); the petrologic tracer of drift ice in the N Atlantic (Bond
942 et al., 2001); the $\delta^{18}O$ and Ca^{2+} records in the Greenland NGRIP ice core indicated air temperature
943 and dust variability on GICC05 age scale (Rasmussen et al., 2014), pollen reconstructed Southern
944 Siberia environment changes (Lake Baikal region) (Bezrukova et al., 2010) and productivity stack
945 for core 41-2. Orange and blue bars are as in Fig. 2. Centennial events with increased productivity
946 are associated with sub-interstadial of the EASM and with increasing input of solar irradiance
947 during the LGM-B/A and EH short-term warmings, respectively. The correlation between short-
948 term increased Greenland temperature (NGRIP ice core) and a decreased Antarctic temperature is
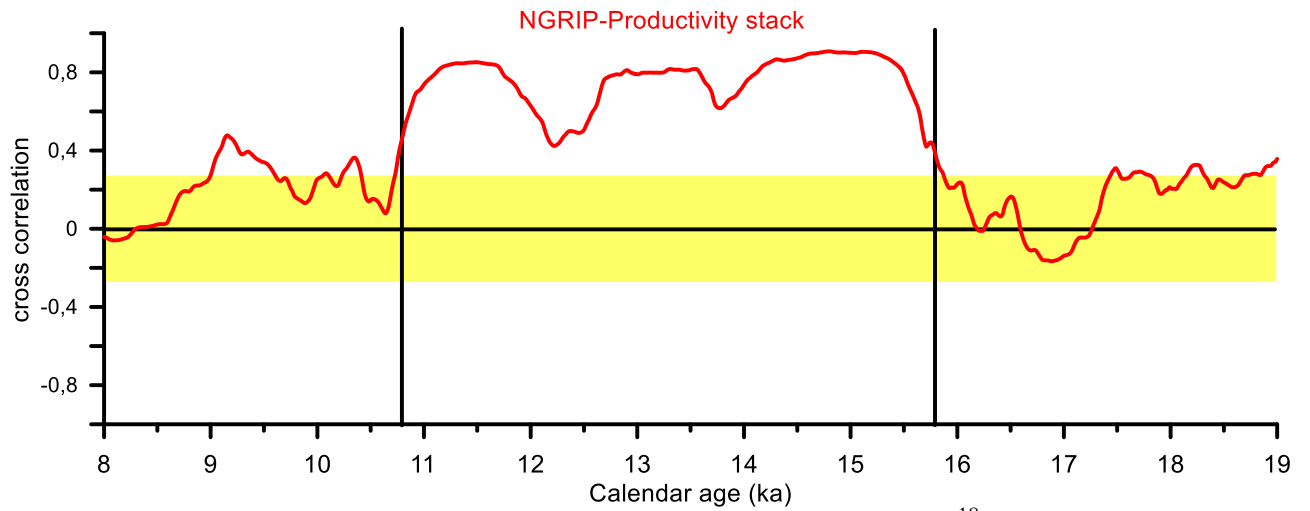949 less pronounced but seems to be marked as well.

950

951

NGRIP-Productivity stack

Fig. 6. Cross correlation (CC) of the NW Pacific productivity stack and $\delta^{18}O$ records of the NGRIP (Rasmussen et al., 2014), using moving windows at 2000 years. Yellow bars depict the CC within range ±0.25. Vertical black lines distinguish an interval from 10.8 to 15.8 ka with significant CC (from -0.6 to -0.9) from less significant CC during earlier and later intervals indicating the synchronicity climate changes between the N Atlantic and NW Pacific.